Neurobiology of Disease

The Stria Vascularis in Mice and Humans Is an Early Site of Age-Related Cochlear Degeneration, Macrophage Dysfunction, and Inflammation

Hainan Lang,[1*] Kenyaria V. Noble,[1*] Jeremy L. Barth,[2*] Jeffrey A. Rumschlag,[1] Tyreek R. Jenkins,[1] Shelby L. Storm,[1] Mark A. Eckert,[3] Judy R. Dubno,[3] and Bradley A. Schulte[1]

[1]Department of Pathology and Laboratory Medicine, Medical University of South Carolina, Charleston, South Carolina 29425, [2]Department of Regenerative Medicine and Cell Biology, Medical University of South Carolina, Charleston, South Carolina 29425, and [3]Department of Otolaryngology-Head and Neck Surgery, Medical University of South Carolina, Charleston, South Carolina 29425

Age-related hearing loss, or presbyacusis, is a common degenerative disorder affecting communication and quality of life for millions of older adults. Multiple pathophysiologic manifestations, along with many cellular and molecular alterations, have been linked to presbyacusis; however, the initial events and causal factors have not been clearly established. Comparisons of the transcriptome in the lateral wall (LW) with other cochlear regions in a mouse model (of both sexes) of "normal" age-related hearing loss revealed that early pathophysiological alterations in the stria vascularis (SV) are associated with increased macrophage activation and a molecular signature indicative of inflammaging, a common form of immune dysfunction. Structure-function correlation analyses in mice across the lifespan showed that the age-dependent increase in macrophage activation in the stria vascularis is associated with a decline in auditory sensitivity. High-resolution imaging analysis of macrophage activation in middle-aged and aged mouse and human cochleas, along with transcriptomic analysis of age-dependent changes in mouse cochlear macrophage gene expression, support the hypothesis that aberrant macrophage activity is an important contributor to age-dependent strial dysfunction, cochlear pathology, and hearing loss. Thus, this study highlights the SV as a primary site of age-related cochlear degeneration and aberrant macrophage activity and dysregulation of the immune system as early indicators of age-related cochlear pathology and hearing loss. Importantly, novel new imaging methods described here now provide a means to analyze human temporal bones in a way that had not previously been feasible and thereby represent a significant new tool for otopathological evaluation.

Key words: cochlea; hearing loss; inflammaging; macrophage; presbyacusis; stria vascularis

Significance Statement

Age-related hearing loss is a common neurodegenerative disorder affecting communication and quality of life. Current interventions (primarily hearing aids and cochlear implants) offer imperfect and often unsuccessful therapeutic outcomes. Identification of early pathology and causal factors is crucial for the development of new treatments and early diagnostic tests. Here, we find that the SV, a nonsensory component of the cochlea, is an early site of structural and functional pathology in mice and humans that is characterized by aberrant immune cell activity. We also establish a new technique for evaluating cochleas from human temporal bones, an important but understudied area of research because of a lack of well-preserved human specimens and difficult tissue preparation and processing approaches.

Received Dec. 5, 2022; revised Apr. 19, 2023; accepted May 25, 2023.

Author contributions: H.L. and K.V.N. designed research; H.L., K.V.N., and T.R.J. performed research; H.L., K.V.N., J.L.B., J.A.R., T.R.J., S.L.S., M.A.E., J.A.R., J.R.D., and B.A.S. analyzed data; H.L. wrote the first draft of the paper; H.L., K.V.N., J.L.B., J.A.R., T.R.J., S.L.S., M.A.E., J.A.R., J.R.D., and B.A.S. edited the paper.

This work was supported in part by National Institutes of Health Grants P50 DC000422 (to H.L., J.R.D., B.A.S.), K18 DC018517 (to H.L.), T32 DC014435 (to K.V.N., T.R.J., J.A.R.), P30 GM103342 (to J.L.B.), and P20 GM103499 (to J.L.B.). Confocal image collection and analysis were done through Medical University of South Carolina (MUSC) Image facilities that were supported in part by the Cell and Molecular Imaging Shared Resource; the MUSC Cancer Center Support Grant P30 CA138313; SC COBRE Grants P20 GM103542 and P20 GM130457; the MUSC Core Center Grant P30 DK123704; and Shared Instrumentation Grants S10 OD018113 and S10 OD028663. Bioinformatic analysis of RNA-seq data was conducted through the MUSC Proteogenomics Facility (supported by P20 GM103499 and the MUSC Office of the Vice President for Research). We thank Nancy Smythe, Cindy Wang, Carlene Brandon, Gang Li, Nathaniel Parsons, Shabih Jafri, Juhong Zhu, and Jiaying Wu for their excellent technical assistance. We also thank Eric Hamlett and many Otolaryngology faculty and residents for their assistance with the collection and processing of human temporal bones. We thank Jayne Ahlstrom, Richard Schmiedt, Price Rainwater, and Federico Luricich for their suggestions and comments on the study and editing of the manuscript.

K. V. Noble's present address: Akouos, Inc., Boston, Massachusetts 02210.

*H.L., K.V.N. and J.L.B contributed equally to this work.

The authors declare no competing financial interests.

Correspondence should be addressed to Hainan Lang at langh@musc.edu.

https://doi.org/10.1523/JNEUROSCI.2234-22.2023

Introduction

Age-related hearing loss, or presbyacusis, is a gradual loss of hearing sensitivity, which negatively impacts communication and quality of life for millions of older adults. Multiple cell types have been reported to be involved in the pathology of presbyacusis, including sensory hair cells, neurons, and glial cells in the auditory nerve (AN; Schuknecht, 1955; Fleischer, 1972; Schuknecht and Gacek, 1993; Ohlemiller et al., 2008; Sha et al., 2008; Makary et al., 2011; Xing et al., 2012; Parthasarathy and Kujawa, 2018; Perkins et al., 2020; P.Z. Wu et al., 2020; H. Liu et al., 2022). The degeneration of non-neural cell types in the stria vascularis (SV) and other regions of the cochlear lateral wall (LW) has also been linked to presbyacusis (Schuknecht, 1964; Schuknecht and Gacek, 1993; Saitoh et al., 1995; Gratton and Schulte, 1995; Kusunoki et al., 2004; Schulte, 2005; Spicer and Schulte, 2005; Ohlemiller et al., 2008; Hao et al., 2014; Carraro and Harrison, 2016; Kurata et al., 2016; Thulasiram et al., 2022; Trpchevska et al., 2022). Although multiple factors are associated with presbyacusis (for review, see Frisina et al., 2016; Keithley, 2020; Eckert et al., 2021), the initial sites of degeneration and drivers of pathophysiology remain unclear.

The SV is a highly metabolically active epithelium with distinct roles critical to supporting auditory function. Multiple cell types in the SV work together to produce the high K^+ concentration in endolymph and generate the endocochlear potential (EP). The mitochondria-rich marginal cells express abundant Na,K-ATPase and Na-K-Cl cotransporter, while intermediate cells express the inwardly-rectifying K^+ channel KIR4.1 (Schulte and Schmiedt, 1992; Tachibana, 1999; Marcus et al., 2002; Schulte, 2005; Korrapati et al., 2019). A dense capillary network within the SV is essential for efficient energy production and formation of the blood-labyrinth barrier, which is regulated via pericytes and/or other mechanisms involving cochlear immune cells (F. Zhang et al., 2013; Shi, 2016; Hirose and Li, 2019; Nyberg et al., 2019). However, this elegantly designed cytoarchitecture makes the SV vulnerable to age-associated pathologic conditions. One of these pathologic conditions, inflammaging, defined by chronic low-grade inflammation with dysregulation of immune cell activity, is increasingly being associated with age-related degenerative disorders (Verschuur et al., 2014; Watson et al., 2017; Franceschi et al., 2018; Bazard et al., 2021).

Macrophages are key elements of the innate immune system and regulate vascular homeostasis in adult tissues (Wenes et al., 2016). Macrophages are present in the adult cochlea in both normal and pathologic conditions (Bohne, 1971; Hirose et al., 2005; Tornabene et al., 2006; T. Ito et al., 2014; Kaur et al., 2015a, b; Frye et al., 2017; Liu et al., 2018; Celaya et al., 2019; Noble et al., 2019; Warchol, 2019; Zhang et al., 2020; Bermúdez-Muñoz et al., 2021). C57BL/6 mice exhibit early-onset hearing loss with significant hair cell loss occurring at approximately three months of age progressing within a short time to a profound hearing loss (Spongr et al., 1997; White et al., 2000). In this strain, cochlear macrophages undergo remarkable morphologic changes (Neng et al., 2015). However, the significant loss of hair cells at an early age makes it difficult to determine the mechanisms underlying the observed changes in macrophage activity and their relationship to cochlear pathology. In contrast, significant loss of hair cells and hearing loss in CBA/CaJ mice does not occur until around 26 months of age (Spongr et al., 1997; Ohlemiller et al., 2010, 2011). Using CBA/CaJ mice, we investigated the extent to which strial degeneration and changes in macrophage activity occur before a significant loss of hair cells. We examined cellular and molecular factors that might contribute to such pathologic alterations, together with the examination of human temporal bones from middle-aged and older donors. Together, the results indicate that the SV is an early site of degeneration and that aberrant macrophage activity is an indication of this degeneration in mice and humans.

Materials and Methods

Mice

All aspects of the animal research were conducted in accordance with the guidelines of the Institutional Animal Care and Use Committee of the Medical University of South Carolina (MUSC). Mouse breeding pairs for CBA/CaJ (stock #JAX000654), C57BL/6J (stock #JAX 000664), and *CX3CR1-GFP* homozygous (*B6.129P2(Cg)-Cx3cr1tm1Litt/J*, stock #JAX 005582; $Cx3cr1^{GFP/GFP}$) mice were purchased from The Jackson Laboratory and bred in a low-noise environment in the Animal Research Facility at MUSC. The CBA/CaJ mouse strain has been used for normal hearing studies because of its lack of genetic mutations related to hearing and its ability to age without progressive hearing loss. Young adult (1.5–3 months), middle-aged (12–18 months), and aged (>24 months) CBA/CaJ mice (of both sexes) were used. Additionally, young adult (1.5–2 months) and aged (10–14 months) *CX3CR1-GFP* heterozygous ($Cx3cr1^{GFP/+}$) mice (of both sexes) were used to perform fluorescence-activated cell sorting (FACS) of macrophages from the cochlea. To generate the *CX3CR1-GFP* heterozygous mice, *CX3CR1-GFP* homozygous animals were crossed with C57BL/6J mice, and the F1 generation of animals were then used for the experiments. Confirmation of mouse mutation status was determined using genotyping procedures modified from The Jackson Laboratory. The sex and number of animals per experimental group are reported in the figure legends or in the Results section. All mice received food and water *ad libitum* and were maintained on a 12/12 h light/dark cycle. Mice with signs of external ear canal and middle ear obstruction or infection were excluded.

CX3CR1-GFP mouse genotyping by PCR

Extraction of tail DNA from each mouse was performed using a two-step HotSHOT extraction protocol. Briefly, 150 μl of Solution 1 (25 mM NaOH, 0.2 mM EDTA) was added to each tissue sample, briefly vortexed, and heated at 100°C for 45 min in a heating block. Following the incubation period, 150 μl of Solution 2 (40 mM Tris HCl, pH 5.5) was added, briefly vortexed then centrifuged, and stored at 4°C until used. Custom DNA oligonucleotides with the appropriate primer sequences [*CX3CR1-GFP* wild-type (WT) forward primer with GTC TTC ACG TTC GGT CTG GT; Common primer with CCC AGA CAC TCG TTG TCC TT; *CX3CR1-GFP* Mutant Forward primer with CTC CCC CTG AAC CTG AAA C] were ordered from either Integrated DNA Technologies or Eurofins Genomics. The target gene of interest was amplified by PCR using the following cycler settings: 94°C for 3 min; 10 cycles of 94°C for 30 s, 65°C for 30 s, 68°C for 1 min; 30 cycles of 94°C for 30 s, 60°C for 30 s, 72°C for 1 min; followed 72°C for 2 min; hold at 10°C. Mice were heterozygous for the CX3CR1-GFP gene locus and exhibited bands for the amplified mutant and WT alleles at 500 and 410 bp, respectively.

Auditory physiology

Cochlear and AN function were measured using the auditory brainstem response (ABR). Averaged recordings provided estimates of ABR Wave I threshold and suprathreshold measurements as in our previous reports in mouse models (Panganiban et al., 2018, 2022). For ABR measurements, both CBA/CaJ mice and WTs and *CX3CR1-GFP* heterozygous mice were anesthetized via an intraperitoneal injection of a cocktail containing 20 mg/kg xylazine and 100 mg/kg ketamine. Auditory tests were performed in a sound-isolation booth.

Equipment for ABR measurements was calibrated before use with TDT RPvdsEx software [Tucker Davis Technologies (TDT)] and a model 378C01 ICP microphone system provided by PCB Piezotronics. In a closed-field setup, sound stimuli were delivered into the ear canal via a 3–5 mm in diameter tube. ABRs were recorded in response to 5-ms tone pips at frequencies of 4, 5.6, 11.3, 16, 22.6, 32, 40, and 45.2 kHz with 0.5 ms $\cos^2$ rise/fall times delivered 31 times/s using a TDT system III

with an RP2.1 enhanced real-time processor. Sound levels were presented from 90–10 dB SPL in 5-dB steps. ABR Wave I thresholds were determined visually for each mouse as the lowest level that elicited a response. Mean and ± SEM thresholds at each frequency across groups were calculated.

Mouse cochlear tissue collection and preparation

Age-related endpoint physiological recordings were taken before the collection of mouse cochleae. Mouse cochleas were collected and immediately fixed with 4% paraformaldehyde (Electron Microscopy Sciences) solution in PBS via cochlear scalae perfusion, then were kept in the same fixative for 1.5–2 h at room temperature. Fixed cochleas were decalcified in 0.12 M EDTA for 48 h then embedded in Tissue-Tek OCT compound and sectioned at a thickness of ~10 µm. For whole-mount preparations, the LWs were isolated from the remainder of the cochlear ducts. Microdissections were performed to isolate the apical, middle, and basal portion of the cochlear LW.

Human cochlear tissue collection and preparation

Procedures for the collection and preparation of human temporal bone samples have been reported previously (Cunningham et al., 2000; Xing et al., 2012; Noble et al., 2019). All the specimens were obtained from the MUSC Hearing Research Program's temporal bone archive and the MUSC Carroll A. Campbell, Jr. Neuropathology Laboratory Brain Bank. In all cases of human temporal bone collection, written and informed consent was obtained from the next-of-kin in accordance with South Carolina laws and regulations. Temporal bone research was approved by the MUSC Institutional Review Board as not human subject research (Pro0030845). After removal of the specimen, scalar perfusion was performed with a 4% solution of paraformaldehyde, and fixation was continued by immersion for at least 48 h. The bones were then rinsed with PBS and decalcified in EDTA for a period of four to six weeks as previously described. Over this period, the specimens were trimmed to remove the hard bone covering the cochlea and vestibular apparatus of the inner ear. The inner ear portions of the trimmed temporal bones were processed for frozen sectioning and whole mount preparations.

Direct immunofluorescent staining on cochlear sections

Cochlear sections were air dried for 10 min, then submerged in ice-cold acetone followed by ice-cold methanol for 5 min each. Sections were permeabilized with 0.2% Triton X-100 for 8 min and then incubated in blocking solution [2% bovine serum albumin (Sigma-Aldrich) in PBS] on a rocker for 1 h. Primary antibody mixes (GAL3 + IBA1, or GAL3 + KIR4.1) were prepared in blocking solution (PBS + 2% BSA) and added to the sections, which were then incubated overnight at 4°C. The following day, sections were washed with PBS, and appropriate fluorescent secondary antibodies (ThermoFisher) were prepared in blocking solution and added to sections for 2 h at room temperature with rocking. Slides were washed with PBS and then mounted with Vectashield (Vector Labs). The primary and secondary antibodies used for immunohistochemistry are listed in Table 1.

Indirect immunofluorescent staining on cochlear sections and whole-mount preparations

Section preparation was the same as described above. For procedures on cochlear sections, staining was performed using biotinylated secondary antibodies conjugated with fluorescent avidin (Vector Labs) as previously described (Lang et al., 2011). For whole-mount preparations, prefixed cochleas were dissected, and the LW tissues were processed into apical, middle, and basal portions. Tissue dehydration was performed by adding increasing concentrations of methanol (25%, 50%, 75%, and 100%) and allowing each to equilibrate for 1 h. Tissue in 100% methanol was kept on ice for 1 h, then placed at −20°C for 4 h. Dent's bleach (4:1:1, MeOH: 30% H_2O_2: DMSO) was added, and the tissue was held at 4°C overnight. Rehydration of the tissue was performed by adding decreasing concentrations of MeOH to the tissue (75%, 50%, and 25%, PBS) allowing each to equilibrate for 10 min. Overnight permeabilization with 1% Triton X-100 was followed by blocking [1% BSA + 10% normal goat serum (EMD Millipore) in PBS] for 2 h. A primary antibody was added and left 24–48 h at 4°C. Samples were washed with PBS, and then species-specific biotinylated secondary antibody (prepared with 2% BSA in PBS) was added to the primary antibody-exposed tissue and incubated overnight at 4°C. Washes with PBS were followed by the addition of fluorescent streptavidin in 0.1 M sodium bicarbonate buffer at pH 8.5 for 2–4 h at room temperature.

Table 1. Antibodies and other histochemical staining related reagents used in the study

Primary antibody	Host	Company	Catalog no.	Concentration
Anti-KIR4.1	Rabbit	Alomone Labs	APC035	1:100
Anti-IBA1	Rabbit	Wako/Abcam	019-19741/	1:200
Anti-GAL3	Goat	R&D Systems	AF1197	1:100
Anti-CD68	Rat	Abcam	Ab53444	1:50
Anti-CD31	Rat	BD Bioscience	553370	1:100
Anti-Na,K-ATPase α-1 subunit	Monoclonal	DSHB	A6F	1:100
Secondary antibody	Host	Company	Catalog no.	Concentration
Biotinylated anti-goat IgG	Horse	Vector Laboratories	BA-9500	1:100
Biotinylated anti-rabbit IgG	Horse	Vector Laboratories	BA-1100	1:100
Biotinylated anti-mouse IgG	Goat	Vector Laboratories	BA-9200	1:100
Anti-biotin dyes	Host	Company	Catalog no.	Concentration
Fluorescein Avidin DCS	N/A	Vector Laboratories	A-2011	1:100
Texas Red Avidin D	N/A	Vector Laboratories	A-2006	1:100
Direct secondary antibodies	Host	Company	Catalog no.	Concentration
Anti-goat Alexa Fluor 568	Donkey	Invitrogen	A11057	1:500
Anti-mouse Alexa Fluor 488	Donkey	Invitrogen	A21202	1:500
Anti-rabbit Alexa Fluor 568	Donkey	Invitrogen	A10042	1:500
Anti-rabbit Alexa Fluor 488	Donkey	Invitrogen	A21206	1:500
Lectin staining	Species	Company	Catalog no.	Concentration
GSA-IB4 Alexa Fluor 488	Mouse	Invitrogen	I21411	1:100
UEA I	Human	Vector Laboratories	FL-1061	1:100

Fluorescent lectin staining with mouse and human strial microvasculature

Some of the section and whole-mount preparations that were stained with IBA1 antibody were also processed for dual staining with lectin using the following procedures. The IBA1 stained LW tissues were washed in PBS and permeabilized with 1 mg/ml saponin (Sigma-Aldrich) + 0.1% Tween 20 overnight at 4°C. The isolectin GSA-IB4 Alexa Fluor 488 conjugate (for mouse tissues; Spicer and Schulte, 1988; Neng et al., 2015; Dufek et al., 2020) or *Ulex europaeus* agglutinin I (UEA I) fluorescein labeled (for human tissues; see Table 1 detailed information) was diluted 1:100 in 0.1% $CaCl_2$ in PBS and incubated with LW tissues overnight at 4°C. Nuclei were counterstained using 4′,6-diamidino-2-phenylindole (DAPI). Tissues were washed and mounted with Vectashield.

Confocal imaging with Airyscan and Imaris analysis

Slice and confocal image stacks were collected using a Zeiss LSM 880 NLO with ZEN acquisition software with Airyscan model (Zeiss United States). For human cochlear section preparations, images were taken at sizes of 340.08 µm (10) × 340.08 µm (y) for evaluating the whole SV and at 166.05 µm (10) × 166.05 µm (y) for evaluating strial cell processes. For mouse cochlear section preparations, images were taken at sizes of 340.08 µm (10) × 340.08 µm (y) for evaluating the whole SV and at 65.89 µm (10) × 65.89 µm (y) for evaluating the strial cell processes. For mouse LW whole-mount preparations, image stacks were taken at 0.94-µm intervals with image sizes of 170.04 µm (10) × 170.04 µm (y). For human LW whole-mount preparations, image stacks were taken at 0.95-µm intervals with image sizes of 425.10 µm (10) × 425.10 µm (y). Images were processed and analyzed using ZEN 2012 Blue Edition (Carl Zeiss Microscopy GmbH) and Adobe Photoshop CC (Adobe Systems Incorporated).

The Imaris volume rendering function (Imaris 9.8, Oxford Instruments; RRID:SCR_007370) was used for 3D reconstruction and analysis of macrophage morphology and interactions between macrophages and strial microvasculature. Mouse LW whole-mount confocal image stacks were first converted to an imaris file (.ims) using ImarisFileConverter. For the 3D reconstruction of macrophages, the "surface" function was applied using the following custom settings: surface detail was defined as 0.650 µm

(smooth); threshold (local contrast) as 560. All reconstructed entities that were clearly not macrophages were manually removed and not included in further analysis. After removal of all nonspecific background signal, the "mask all" function was used to create the final surface reconstruction. Next, the "surface" reconstruction was used as the template for adding the "filament" (GSA-IB4$^+$ strial microvasculature) reconstruction using the following custom settings: largest diameter as 14.1 μm; thinnest diameter as 0.995 μm; seed point threshold was set as 1453. All surface and filament parameters were exported into a separate Excel file.

Persistent homology analyses for whole-mount preparation

Persistent homology is an algebraic topology method for characterizing the shape of data (Edelsbrunner et al., 2000), including histologic imaging data (Lawson et al., 2019). More specifically, two-dimensional histologic images of the strial microvasculature and macrophages can be characterized based on (1) the number of components (zero-cycle) or extent of stained tissue, as well as (2) loops (one-cycle) that appear in the network of connected branching capillaries and in activated macrophages that have a ringed ameboid appearance (Fig. 2*G*,*H*). This quantification is achieved through a filtration across a dimension of an image (e.g., image contrast or space). Here, a spatial filtration was performed (Garin and Tauzin, 2019) to identify boundaries of vessels or macrophages where they were first encountered (birth) and merged (death) across the space of a histologic section.

The persistent homology analyses were performed using Python (v 3.7). Zeiss (CZI) formatted histologic data were read in Python using the CziFile library (v 2019.7.2), contrast thresholded to remove background noise (for eight-bit converted data: strial vasculature > 55; macrophages > 90), and Gaussian filtered ($\sigma = 6$) using the SciPy library (1.7.3) to remove small noisy voxels with higher contrast values. Image sections were then binarized using the Giotto-tda Binarizer function (v 0.5.1). This binarization step allowed for a height filtration of the images using the Giotto-tda HeightFiltration function. Persistent homology was then performed across the space of the image to identify zero-cycle components and one-cycle loops in strial microvasculature and macrophage data using the Rips cubical complex approach from the Gudhi library (v 3.0.0). These zero-cycle components and one-cycle loops are represented in a persistence diagram, where the difference between birth values along the unity line and death values away from the unity line reflects how long the structure persisted or was present across the image. Persistence diagrams were produced using the matplotlib scatter plot function (v 3.1.1) to demonstrate the unique patterns of microvasculature and macrophage anatomy across mouse and human cases (as represented by the birth and death values of their components and loops). Symbols in these diagrams that fall along the unity line were small structures that did not persist across the space of an image. Symbols falling away from the unity line were larger structures. We direct the reader to the one-cycle loop structures in these diagrams that are far from the unity line and represent branching capillaries or activated macrophages that occupied space across an image.

Mouse strial thickness, macrophage measurements and determination of the interactions between macrophages and strial microvasculature

Images were taken of cross-sectional areas of the SV in the middle turn using a fluorescent microscope (Zeiss Axio Observer). Activated macrophages stained with GAL3 were outlined using the classification tool in Image Pro Plus software (Image Pro Plus software 6.0). The entire SV also was outlined. All measures avoided regions of the SV cut tangentially. The macrophage areas were summed and divided by the SV area to determine the percent of the SV cross-sectional area occupied by activated macrophages. Measures of SV thickness were taken at three locations randomly selected and averaged. To assess interactions between macrophages and microvasculature, we determined the number of macrophage processes that were in close proximity (associated with) capillaries (i.e., macrophages were counted based on whether there were more than or equal to two associations or less than two associations; Fig. 2*I*,*J*). Although the level of interaction between macrophages and the strial microvasculature was not directly measured, "an interaction" was considered to occur when more than two processes from an IBA1$^+$ macrophage were in contact with a capillary (Figs. 2*F*, left panel, 2*I*, 5*H*), and "no interaction" was determined when fewer than two processes per IBA$^+$ macrophage were seen in close proximity to a capillary (Fig. 2*F*, right panel, 2*J*).

Human strial macrophage, strial thickness, and microvasculature measurements

Images were taken of cross-sectional areas of the SV in the middle turn using Zeiss LSM 880 as described earlier. Each confocal image was analyzed to count the number of activated macrophages using a tool in the Measure function (Image Pro Plus software 6.0) to outline regions on the images. Only IBA1$^+$ macrophages with a round soma measuring over 8 μm in diameter were counted as activated macrophages. The 8-μm threshold was determined based on preliminary observations of the sizes of "ramified" macrophages in strial whole-mount preparations stained with IBA1 and cochlear sections stained with GAL3, an activated macrophage-marker. Small processes or dendritic-like macrophages were not counted as these are not considered to be activated. Measures of SV thickness were taken at three locations randomly selected per cochlear section in the middle region of the cochlea and averaged. All counts avoided regions where the SV was cut tangentially. The number of UEAI$^+$ strial microvasculature in cross-section on each image was also counted using the classification tool in Image Pro Plus software (Image Pro Plus software 6.0).

Transmission electron microscopy

Samples were prepared for transmission electron microscopy (TEM) using procedures modified from a previous publication (Lang et al., 2015). Briefly, deeply anesthetized mice were cardiac perfused with a mixture of 10-ml saline and 0.1% sodium nitrite solution followed by 15 ml of a fixative solution containing 4% paraformaldehyde and 2% glutaraldehyde in 0.1 M phosphate buffer, pH 7.4. The same fixative solution was used to perfuse the excised cochleae through the round window and for further immersion overnight at 4°C. Cochleae were then decalcified using 0.12 M EDTA solution at room temperature for 2–3 d with a magnetic stirrer. Then, cochleae were fixed using a solution containing 1% osmium tetroxide and 1.5% ferrocyanide for 2 h in the dark. They were then dehydrated and embedded in Epon LX 112 resin. Semi-thin sections for pre-TEM observation of AN orientation were cut at 1 μm-thickness and stained with toluidine blue. Once a cochlear apical, middle, or basal plane was identified, ultrathin sections at 70-nm thickness were cut and stained with uranyl acetate and lead citrate. These ultrathin sections were examined with a JEOL JEM-1010 transmission electron microscope (JEOL USA).

Total RNA preparation from cochlear tissues

Cochleae were collected following endpoint auditory physiology measures. Microdissections were performed to isolate LW and AN (including sensory epithelium; see Fig. 1*E*), taking care to preserve tissue integrity. Individual samples consisted of the tissues collected from a single mouse (i.e., the two cochlea) pooled together. Purification of total RNA from each sample was performed using either the miRNeasy Mini kit (QIAGEN) or the RNeasy Plus Micro kit (QIAGEN) per manufacturer instructions. Quality of each total RNA isolation was assessed using the Agilent 2100 Bioanalyzer; low-quality samples displaying degradation or contamination were excluded.

Microarray analysis of aging effects in AN and LW at 18 months

Gene expression in AN and LW was evaluated by microarray analysis using Mouse Genome 430 2.0 GeneChips (ThermoFisher Scientific). Three biological replicates of AN and LW young adult (1.5–3 months) and middle-aged adult (18 months) samples from CBA/CaJ mice were used. Microarray sample preparation, hybridization and scanning were done as described previously (Panganiban et al., 2018). Raw data (CEL files) were processed as a group using Applied Biosystems Transcriptome Analysis Console version 4.0.2 (ThermoFisher Scientific). Data were summarized by robust multiarray average (RMA), and young adult and middle-aged samples for each tissue type were compared using false discovery rate (FDR; $p < 0.05$) adjusted p-values to define significant effects of probe sets. Significant difference was assigned for probe sets with FDR adjusted p-value < 0.05. Significantly different probe sets were further refined by

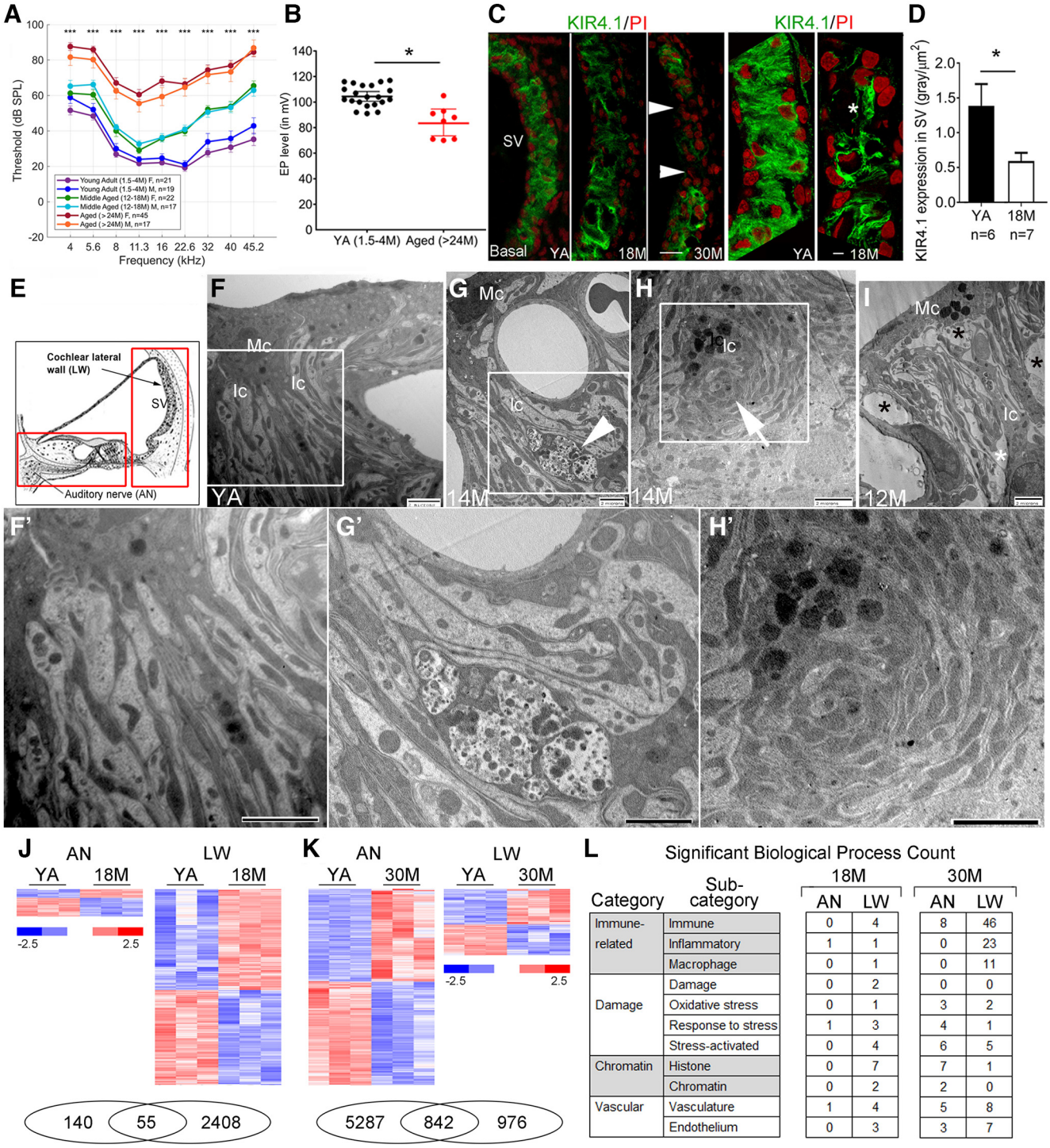

Category	Sub-category	18M AN	18M LW	30M AN	30M LW
Immune-related	Immune	0	4	8	46
	Inflammatory	1	1	0	23
	Macrophage	0	1	0	11
Damage	Damage	0	2	0	0
	Oxidative stress	0	1	3	2
	Response to stress	1	3	4	1
	Stress-activated	0	4	6	5
Chromatin	Histone	0	7	7	1
	Chromatin	0	2	2	0
Vascular	Vasculature	1	4	5	8
	Endothelium	0	3	3	7

Figure 1. Age-related strial pathology and changes to the inflammaging-related genes in the stria vascularis of CBA/CaJ mice. ***A***, Auditory brainstem response (ABR) thresholds of 24- to 30-month (M)-old CBA/CaJ mice were elevated when compared with 12- to 18-M-old and 1.5- to 4-M-old mice. There are 19 males and 21 females in the young adult group, 17 males and 22 females in the middle-aged group, and 17 males and 45 females in the aged group. Data are presented as mean ± SEM. ***B***, Age-related EP reduction in aged mice. Data are presented as mean ± SEM (young adults: $n = 21$, 10 males; aged: $n = 8$, 3 males). ***C***, The three left panels show changes in KIR4.1 (green) immunoreactivity in strial intermediate cells (Ic) of both middle-aged and older mice. Arrowheads indicate a total loss of KIR4.1$^+$ Ics in a 30-M-old mouse. Super-resolution confocal images in the two right panels reveal a reduction of KIR4.1 (asterisk) immunoreactivity in the SV of a middle-aged mouse. ***D***, Quantitative analysis showing a significant reduction in KIR4.1 immunoreactivity in the middle-aged group. Data are presented as mean ± SEM (*$p < 0.05$, Mann–Whitney *U* test). ***E***, A schematic illustration of the cochlea indicates the SV in the cochlear lateral wall (LW) and the auditory nerve (AN). The boxes indicate the cochlear regions of the LW and the AN including sensory epithelium that is isolated for gene expression analysis. ***F***, Ultrastructural analysis of the SV in a young adult mouse shows the normal cellular processes between the strial marginal cells (Mcs) and Ics. ***G–I***, Several pathologic alterations related to the interdigitating processes were seen in the SVs of middle-aged mice. A portion of a macrophage-like cell is present among the processes of the Mc and Ic (***G***; arrowhead). Degenerating Ic processes (***H***; arrow) are seen in a 14-M-old mouse. Increased intrastrial space appears in a 12-M-old mouse (***I***; asterisks). Images in ***F′***, ***G′***, and ***H′*** are enlarged images of the boxed regions in ***F***, ***G***, and ***H***, respectively. Scale bars: 20 μm in ***B***, 5 μm in ***C***, 2 μm in ***F–I*** and ***F′–H′***. ***J***, ***K***, Transcriptomic analysis comparing young adult (YA) to middle-aged (***J***) and aged (***K***) groups identified differentially expressed genes in both AN and LW samples (Extended Data Fig. 1-1). At each age group there is an overlap in genes differentially expressed in the two tissues (Venn diagrams shown at bottom). ***L***, Tabulation of significant transcriptomic enriched biological processes relating to aspects of inflammaging (immune response, damage, chromatin alteration, and vascular function; Extended Data Fig. 1-2). At 18 M, the number of enriched biological processes relating to immune response and damage are elevated in LW compared with AN; at 30 M, the numbers for immune response categories are again elevated in the LW.

eliminating redundant gene representations and probe sets not corresponding to known genes. This yielded 195 genes differentially expressed in AN and 2463 genes differentially expressed in LW in middle-aged samples, compared with respective young adults. Raw and processed microarray data are archived in NCBI Gene Expression Omnibus (AN, Dataset GSE121856; LW, Dataset GSE98070).

RNA-seq analysis of aging effects in AN and LW at 30 months

RNA-seq analysis of aged AN has been described previously (Panganiban et al., 2022; NCBI GEO Dataset GSE141865). For LW, three biological replicates of young adult (two months) and aged adult (30 months) samples from CBA/CaJ mice were analyzed. Each RNA sample combined two to six cochleas isolated from individual mice, and included both male and female animals. Sample processing and sequencing were conducted at the Hollings Cancer Center Genomics Shared Resource facility at MUSC. Libraries were prepared using the TruSeq RNA Library Prep kit (Illumina) and sequencing was performed using an Illumina HiSeq 2500. Resulting fastq files were analyzed using Partek Flow software. Alignment was done with TopHat2 using mouse genome mm10 and data were quantified to annotation model (Partek E/M) using mm10 RefSeq transcripts with the limits: (1) strict paired-end compatibility, (2) require junction reads to match introns, (3) minimum read overlap with feature at 100% of read length, and (4) minimum reads of 10. Normalization and comparison were done by DESeq2 (Love et al., 2014), which calculates an adjusted *p*-value (FDR step up). Significant difference between young adult and aged AN or LW samples was defined as *p*-adjusted < 0.05. This yielded 6129 genes for AN and 1818 genes for LW. Raw and processed data for the aged LW study are archived in NCBI Gene Expression Omnibus (accession GSE197634).

Analysis of transcriptomic data to assess inflammaging in AN and LW

Relative inflammaging effects in middle-aged or aged AN and LW were assessed by counting significantly enriched biological process gene ontologies. Biological processes significantly enriched in AN or LW of middle-aged or aged samples were obtained by ToppGene (Chen et al., 2009) analysis of differentially expressed gene sets described earlier. Significantly enriched (Benjamini and Hochberg FDR adjusted *p*-value < 0.05) biological process titles were searched for select text terms indicative of processes associated with inflammaging: immune function ("immune," "inflammatory," "macrophage"), damage ("damage," "oxidative stress," "response to stress," "stress-activated"), chromatin ("histone," "chromatin"), and vascular function ("vascul," "endothel").

FACS of mouse cochlear macrophages

Macrophages and nonmacrophages were isolated from young adult (1.5–2 months) and older adult (12–14 months) *CX3CR1*$^{GFP/+}$ mouse cochleas (AN + LW, $n = 1$ mouse per sample) or cochlea substructures (AN or LW, $n = 3$ mice per sample). Cells collected from a single mouse were treated as an independent biological sample. Cochleas of *CX3CR1*$^{GFP/+}$ mice were subjected to micro-dissection in cold HBSS solution for the isolation of AN and cochlear LW tissues. All isolation procedures, other than incubation and centrifugation, were performed in a laminar flow hood (a Class II biosafety cabinet). Samples were then transferred into 4-well plates containing a prewarmed ($\leq$5 min at 37°C, 5% CO_2) enzymatic digestion solution (150 µl per sample) consisting of 0.5 mg/ml collagenase (Sigma, catalog #C-1764) and 0.2% trypsin incubated at 37°C for 7 min; 150-µl DNase I (1 mg/ml) was added, and the mixture was triturated three times and then returned to the incubator for 7 min; 300 µl of 10% fetal bovine serum (FBS) in DMEM was added to each well to quench the enzymatic digestion, the cells were triturated 40–50 times using a 200-µl pipette to break up clumps and aid tissue dissociation, and the mixture was transferred to a 15 ml conical tube (600 µl of combined digestion solution, DNase I, and 10% FBS in DMEM). An additional 300 µl of 10% FBS in DMEM was added to the wells to collect any remaining cells, and this volume was transferred to the 15-ml tube. Samples were centrifuged at 1800 rpm for 5 min at room temperature, supernatant was aspirated, and the cell pellet resuspended in 300 µl of FACS buffer (10 mM HEPES, 0.5% BSA and 5 mM EDTA in PBS with pH 7.4). Samples were centrifuged for a second time at 1.8k rpm for 5 min at room temperature, the supernatant was aspirated, and the cell pellet resuspended in 400 µL FACS buffer. The cell suspension was passed through a 0.2-µm filter top polystyrene tube for each sample. The 15-ml conical vial was rinsed with an additional 200 µl of FACS buffer and this volume was filtered through the filter tube. To label dead cells, 1 µl of propidium iodide (PI) was added to the PI compensation control sample (200-µl aliquot of WT cells incubated in the freezer for 5 min) and to all the samples intended for sorting. No PI was added to the GFP compensation control or the unstained compensation control sample. All samples and FACS buffer were held on ice until sorting was performed using a FACSAria Ilu cell sorter for the enrichment of GFP$^+$ cells. The FACSAria Ilu cell sorter is controlled by an HP xw4600 workstation running FACSDiva version 6.1.3.

RNA-seq analysis of macrophage-enriched and age-dependent gene expression

Macrophages and nonmacrophages were isolated (as described in a previous section) from young adult (1.5–2 months) and aged (12–14 months) *CX3CR1*$^{GFP/+}$ mouse cochlea tissues. Total RNA was prepared using the RNeasy Micro kit (QIAGEN), and the quality of each preparation was assessed by 4200 TapeStation, with low-quality samples excluded from further analysis. For RNA-seq analysis, the sample types and biological replicates were as follows: young adult cochlea macrophage ($n = 2$); young adult cochlea nonmacrophage ($n = 4$); young adult AN macrophage ($n = 1$); young adult AN nonmacrophage ($n = 1$); young adult LW macrophage ($n = 1$); young adult LW nonmacrophage ($n = 1$); aged adult cochlea macrophage ($n = 4$); aged adult cochlea nonmacrophage ($n = 4$). Libraries were prepared using the SMARTer Ultra Low + Nextera XT kit (Illumina). Paired-end sequencing was performed on an Illumina HiSeq 2500 using Rapid Run mode at 1 × 50 cycles. A subset of sample libraries was sequenced a second time to increase depth. Sequence data were processed as described earlier for the aged study of AN and LW in CBA/CaJ mice. For comparative analysis with DESeq2, comparisons were limited to sample types with multiple replicates, namely, (1) young adult cochlear macrophages versus nonmacrophages and (2) aged adult cochlear macrophages versus young adult cochlear macrophages. Enriched expression in young adult macrophages versus nonmacrophages was defined as *p*-adjusted < 0.05 and fold change increase > 2. Significant difference between young adult and aged adult macrophages was defined as absolute fold change > 2 and *p*-adjusted < 0.05. Raw and processed data from for the entire study are archived in NCBI Gene Expression Omnibus (accession GSE198345).

Statistical analyses

Sample sizes for physiological experiments and morphologic observations are listed in the appropriate Results section and figure legends. Images presented herein are representative of each experimental group for fluorescence staining or *in situ* hybridization. Quantitative data were evaluated for normality using either Shapiro–Wilk or Kolmogorov–Smirnov tests followed by statistical analysis with the appropriate parametric or nonparametric tests. For Mann–Whitney *U* tests, simple linear regression analyses, and nonparametric mixed-design ANOVA (Wald Type III; Bates et al., 2015), a *p*-value of ≤ 0.05 was considered significant. For differential expression analyses of the RNA-seq datasets, a *p*-adjusted value (FDR step up) of ≤ 0.05 was considered significant. Statistical software and packages used in this project include DeSeq2 (Love et al., 2014), Microsoft Excel, R version 3.5.2, or GraphPad Prism 8 (GraphPad Software).

Results

Age-related pathology and inflammaging-related gene dysregulation in the SV of middle-aged and aged CBA/CaJ mice

ABR Wave I thresholds were significantly elevated in aged CBA/CaJ mice when compared with middle-aged ($F_{(1,97)} = 35.482$, $p < 0.001$; LMER:ANOVA Type III) and young adult mice ($F_{(1,97)}$

= 67.755, $p < 0.001$; LMER:ANOVA Type III); Fig. 1*A*). Mild threshold shifts in lower and middle-range frequencies and moderate threshold shifts in higher frequencies were seen in the middle-aged group, whereas larger threshold shifts were seen across all frequencies in aged mice. No significant differences in ABR thresholds were observed between male and female mice within the young adult group (19 males and 21 females; $F_{(1,19)} = 0.400$, $p = 0.675$), the middle-aged group (17 males and 22 females; $F_{(1,23)} = 0.021$, $p = 0.886$), or the aged group (17 males and 45 females; $F_{(1,31)} = 0.313$, $p = 0.580$; LMER:ANOVA Type III). The EP was also significantly diminished in aged mice compared with young adult mice ($p = 0.0003$; Mann–Whitney *U* test; 21 young adults including 10 males and 11 females; eight aged mice including three males and five females; Fig. 1*B*). These results are in agreement with prior studies that found significant loss of strial marginal cells and outer sulcus cells in aged CBA/CaJ mice (Ohlemiller et al., 2010). Few observations of reduced EP have been reported in CBA/CaJ mice younger than 18 months of age. Although our study did not measure EP in middle-aged mice, the immunostaining data showed an unexpected significant decline in immunoreactivity for the inwardly rectifying potassium channel 4.1 (KIR4.1), a strial functional marker essential to maintaining the high K^+ concentration in endolymph (Liu et al., 2019), in this age group. A significant reduction of KIR4.1 immunoreactivity was seen in the basal turns of the cochlea of middle-aged mice ($p = 0.0256$; Mann–Whitney *U* test; Fig. 1*B–D*). In contrast, in this same group of middle-aged mice, no significant change in strial thickness was found in the basal turns (28.89 ± 2.76 µm, $n = 7$, four males) as compared with young adult mice (29.95 ± 6.58 µm, $n = 6$, 2 males; $p = 0.21$, Mann–Whitney *U* test). In addition, TEM analysis detected several alterations in the SV of middle-aged mice, including a change in the interdigitation pattern between strial marginal and intermediate cells (Fig. 1*F–I*,*F'*,*G'*,*H'*). In young adults, extensive membrane interdigitation (Fig. 1*F*,*F'*) occurred between electron dense marginal cell processes containing abundant mitochondria and more electron-lucent intermediate cell processes. This structural arrangement maximizes the surface area for the ion exchange needed to generate and maintain the EP (Tasaki and Spyropoulos, 1959). Pathologic alterations observed in strial interdigitation-related structures in middle-aged mice included: (1) the appearance of macrophage-like cells between marginal and intermediate cells (Fig. 1*G*,*G'*), (2) abnormal strial cell processes with "whorl"-like shapes (Fig. 1*H*,*H'*), and (3) enlarged spaces between the processes (Fig. 1*I*). Some of these pathologic alterations have been reported previously in aged gerbils (Spicer and Schulte, 2005). Our TEM analysis was conducted with four middle-aged mice (two males) and five young adults (three males). Pathologic alterations in the SV were identified in the middle portion of the cochleas from all four middle-aged mice, but not in the five young adult mice examined in this study. These findings identify the SV as a site of early deterioration related to the onset of age-related hearing loss. Our observations further suggest that immunostaining with markers of strial function (such as KIR4.1, Na^+,K^+-ATPase, and NKCC) provides a sensitive approach for identifying functional changes that are not detected by measurements of strial thickness exclusively.

To further test the hypothesis that the LW is an early site of age-related cochlear degeneration, gene expression analysis of LW and AN (including sensory epithelium) samples from middle-aged and aged mice was performed (Fig. 1*J–L*). Transcriptomic analysis found that tissues from both LW and AN exhibited significant changes in gene expression by middle age with the number of genes affected in the cochlear LW being notably higher (2463 in cochlear LW vs 195 in AN; Fig. 1*J*,*K*; significant difference was assigned for probe sets with FDR adjusted p-value < 0.05 for gene array analysis; see the detailed information in Extended Data Fig. 1-1). Analysis of tissues from aged mice again found that LW and AN exhibited significant age-related changes in gene expression but with the number of genes affected being larger in the AN (6129 in AN vs 1818 in LW; significant difference was defined as p-adjusted < 0.05 for RNA-seq analysis; see the detailed information in Extended Data Fig. 1-1). To directly compare age-related effects between the two sites, we evaluated biological processes enriched among the differentially expressed genes with a focus on several key processes related to inflammaging (Franceschi et al., 2018; Mészáros et al., 2020). Specifically, we counted the number of enriched gene ontology categories relating to immune function, damage, chromatin, and vascular function (Fig. 1*L*). The results demonstrated that these inflammaging categories are elevated in the LW compared with the AN, particularly in the middle-aged group. In middle-aged mice, AN samples showed enrichments in only three inflammaging categories, whereas 32 categories were affected in the LW, corresponding to an ~10:1 increase (Fig. 1*L*; Extended Data Fig. 1-2). In the aged mice, there was more balance between AN and LW in most of the inflammaging categories. However, the immune-related category was substantially higher in the LW (Fig. 1*L*). These gene expression results were supported by TEM examination and immunohistochemistry showing SV pathology in the middle-aged group (Fig. 1*B–I*).

Degeneration of strial microvasculature in middle-aged and aged CBA/CaJ mice

A feature of age-related change in the SV is the degeneration and loss of strial capillaries (Schuknecht and Gacek, 1993; Gratton and Schulte, 1995; Suzuki et al., 2016). Pathologic alterations in rodent models of age-related hearing loss include a reduction of strial capillary density in C57BL/6 mice (Neng et al., 2015; Carraro and Harrison, 2016) and a partial to complete loss of capillaries in both the apical and basal regions, with the middle turn largely spared in gerbil cochleas (Gratton and Schulte, 1995). Here, we characterized age-related microvascular degeneration in middle-aged and aged CBA/CaJ mice using a combination of immunostaining for the endothelial marker CD31 and/or histochemical detection of Isolectin GSA-IB4. A substantial loss of microvasculature network density was found in the apical SV of aged versus young adult mice (Fig. 2*A*). These effects were detected as early as 12 months in the apical SV (Fig. 2*A*), based on the appearance of enlarged capillaries (with a diameter of 12–16 µm) and a reduced number of small (4–6 µm) and middle (8–10 µm) sized capillaries. These whole-mount preparations were conducted in eight young adult mice (four males), six middle-aged mice (two males), and nine aged mice (three males). These specimens were also stained with IBA1 as shown in Figure 2*E*,*F*. To better understand the observed strial microvasculature pathologies, we examined the expression profiles of vascular function genes identified as transcriptionally regulated in the LW of middle-aged and aged CBA/CaJ mice (Fig. 1*L*). Of the 630 genes detected in middle-aged mice (Fig. 2*B*, left panel) and the 200 genes detected in aged mice (Fig. 2*B*, right panel), 51 were affected at both age groups (Extended Data Fig. 2-1). Among these, downregulated genes included *Type I Collagen α2* (*Col1a2*), *Semaphorin 5A*

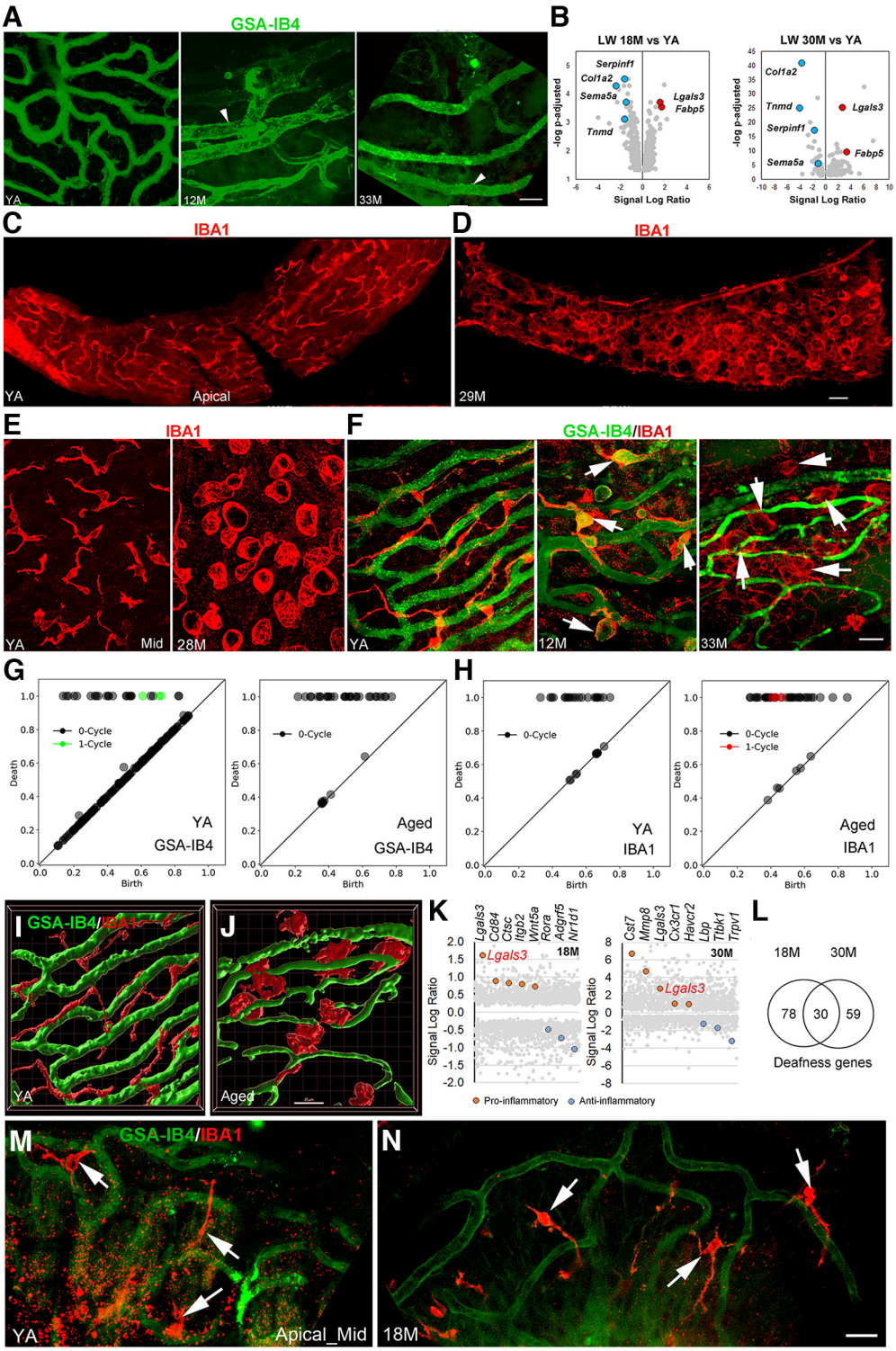

Figure 2. Age-related strial microvasculature and macrophage alterations and associated gene expression changes in middle-aged and aged CBA/CaJ mice. ***A***, Isolectin GSA-IB4 (from *Griffonia simplicifolia*, Alexa Flour 488 conjugate) stained strial capillaries in the apical turn of young adult (YA; left panel), middle-aged (middle panel), and aged (right panel) mice. Enlarged capillaries (arrowheads) were seen in the apical SV in both middle-aged and aged mice. ***B***, Volcano plots of vascular function genes in the LW of middle-aged (left panel) and aged (right panel) mice (Extended Data Fig. 2-1). Selected upregulated (red) and downregulated (blue) genes are highlighted; values for other genes are shown in gray. Note that *Lgals3* was identified as differentially expressed in the LW of both middle-aged and aged CBA/CaJ mice. ***C–E***, Macrophages in the SV undergo dramatic alterations in morphology in aged mice. ***F***, High-resolution images reveal age-related changes in macrophage morphology and macrophage-capillary interactions in the SV of middle-aged (middle panel) and aged mice (right panel). ***G***, ***H***, Persistent homology analyses were performed using images of whole-mount preparations (right and left panels in ***F***) to quantify the distinct GSA-IB4^{+} microvascular (***G***) and IBA1^{+} macrophage (***H***) structural profiles in YA and aged mice. Diagrams show more one-cycle loop structures in the microvasculature of YA compared with aged mouse. In contrast, the increase in one-cycle loops in the aged mouse (***H***, left panel) indicates a greater number of activated macrophages with ringed ameboid appearance compared with YA (***H***, right panel). The *x*- and *y*-axes show relative units after scaling to maximal death value from each analysis. ***I***, ***J***, 3D reconstruction images generated by Imaris 3D volume rendering highlight morphologic changes in macrophages (red) of aged mice that are associated with strial microvasculature (green). Images were generated from Z-stacks of ***F***, left and right panels, respectively. ***K***, Transcriptomic data for LW from middle-aged and aged mice as compared with YA controls. Genes related to macrophage activation that are proinflammatory (red) or anti-inflammatory (blue) were differentially expressed in middle-aged (left

(*Sema5a*), *Serpin Family F Member 1* (*Serpinf1*), and *Tenomodulin* (*Tnmd*). *Col1a2* is a structural component of blood vessels (Gorący et al., 2020; Zheng et al., 2021), and *Serpinf1* has both an anti-inflammatory and immunoregulatory role (Ma et al., 2021); *Sema5a and Tnmd* are angiogenesis regulators (Shukunami et al., 2005; Sadanandam et al., 2010). Upregulated genes included fatty acid binding protein 5 (*Fabp5*) and a lectin, galactose binding soluble 3 (*Lgals3*). *Fabp5* is an intracellular lipid transporter that has proangiogenic effects (Yu et al., 2016; Pan et al., 2018) and is linked to macrophage programming (El Kharbili et al., 2022) and to numerous human pathologic conditions (Smathers and Petersen, 2011; Xu et al., 2022). *Lgals3* encodes Galectin3 (GAL3), which is a β-galactoside-binding lectin that plays an important role in numerous cellular functions such as cell-cell adhesion, angiogenesis, apoptosis, and macrophage activation (Henderson and Sethi, 2009; Sciacchitano et al., 2018) and its dysregulation has been linked to pathologic conditions that include age-related disorders (Sciacchitano et al., 2018; Puigdellívol et al., 2020).

Age-related functional changes in macrophages in the LW of CBA/CaJ mice

Aging is a complex process that may involve pathologic alterations in multiple cell types at several levels. Increasing evidence supports the view that such pathologic alterations are attributable to inflammation (Franceschi et al., 2000; Fulop et al., 2018). Because our transcriptomic analysis detected an enhancement in immune-related processes occurring in the LW as early as middle age (Fig. 1*J–L*), we tested the hypothesis that macrophage dysfunction is associated with degeneration of the strial microvasculature in middle-aged and aged mice. Ionized calcium binding adaptor molecule 1 (IBA1) is a microglia/macrophage-specific calcium-binding protein and has been widely used as a marker of tissue macrophages (including both resident and infiltrated cells; Imai et al., 1996; Ito et al., 1998; Ohsawa et al., 2004). As a key component of the innate immune system, macrophages can be indicators of inflammatory status in the LW. Nonactivated macrophages ("resting" macrophages) are in a surveillance mode to monitor the surrounding environment and have a highly branched morphology with a small soma ("ramified" macrophages). In contrast, activated macrophages often withdraw their processes and assume an "amoeboid" shape. Morphologic alterations of macrophages and their interactions with the strial microvasculature were first examined by dual staining using anti-IBA1 for macrophages and isolectin GSA-IB4 for the microvasculature in whole-mount preparations of the LW (Fig. 2*C–J*). In young adult mice, macrophages in the SV extended multiple elongated cellular processes (ramified shape) and localized in close proximity to the strial microvasculature (Fig. 2*F*, left panels). In middle-aged mice, some of the strial macrophages appeared more rounded and were less closely associated with strial capillaries (Fig. 2*F*, middle panel). These differences in morphologic complexity were quantified using persistent homology, which showed a more looping vascular structure and a more looping ameboid macrophage structure in younger and older mice, respectively, as seen in (Fig. 2*G*,*H*) and Imaris 3D volume rendering (Fig. 2*I*,*J*). The results clearly illustrate a loss of microvasculature, macrophage processes, and macrophage-capillary interactions in aged CBA/CaJ mice compared with the young controls. In contrast, no significant alterations in macrophage morphology or their interactions with the microvasculature were identified in the AN region of middle-aged cochleas (Fig. 2*M*,*N*).

In many pathologic conditions, activated microglia/macrophages assume an amoeboid shape with few or no extended cellular processes (Aloisi, 2001), which allows greater mobility to reach and phagocytose dying cells or cellular debris. These activated macrophages often signal cytokine activation pathways that rapidly stimulate neighboring immune cells to secrete cytokines and enhance inflammation. To further test the hypothesis that age-related activation of macrophages is associated with increased cochlear inflammation, we re-examined our LW transcriptomic data in middle-aged and aged CBA/CaJ mice, focusing on genes that affect macrophage activation. Several macrophage activation genes that are proinflammatory were upregulated in middle-aged and aged mice. These included *Lgals3* (identified earlier in Fig. 2*B* as a differentially expressed vascular function gene) at both ages, as well as *Cd84*, *Ctsc*, *Itgb2*, and *Wnt5a* in the middle age LW, and *Cst7*, *Cx3cr1*, *Havcr1*, and *Mmp8* in the aged LW (Fig. 2*K*; Extended Data Fig. 2-2). Conversely, several genes that regulate macrophage activation and are anti-inflammatory were downregulated, such as *Rora*, *Adgrf5*, and *Nr1d1* in middle age LW, and *Lbp*, *Ttbk1*, and *Trpv1* in aged LW. Nr1d1 plays a protective role in vascular tissue via regulation of inflammation (Wu et al., 2021). LBP (the protein encoded by *Lbp)* is a regulator of inflammation and a promoter of macrophage survival (Sallam et al., 2014). We further queried the LW transcriptomic data for genes linked to deafness (or hearing loss) using a reference list of ~700 genes found to be associated with human deafness (Lewis et al., 2022). We found that 108 and 89 of these genes were significantly affected in middle-aged and aged LW, respectively (Fig. 2*L*; Extended Data Fig. 2-3). Interestingly, *Lgals3* is also one of the deafness-associated genes. Collectively, these results suggest that (1) dysregulation of macrophage activity occurs in the aged SV, and (2) increased macrophage activation in the SV of the middle-aged mice may be an early indicator of cochlear inflammation.

Increased macrophage activation in the SV coincides with auditory function declines in aged CBA/CaJ mice

Morphologic features of macrophage activation as described earlier for "resting" and "ramified" macrophages can be used as biomarkers of cochlear inflammation. To better understand the role of *Lgals3* in the LW of aging CBA/CaJ mice, dual immunostaining was performed for GAL3 (the protein encoded by *Lgals3*) with either IBA1 (Fig. 3*A*), KIR4.1 (intermediate cells; Fig. 3*B–D*), CD68 (Fig. 3*H–J*), or Na,K-ATPase (marginal cells; Fig. 3*K*). Consistent with our gene expression findings, very few IBA^+/$GAL3^+$ cells were observed in the SV of young adult mice, while IBA^+/$GAL3^+$ cells were frequently seen in the aged SV (Fig. 3*A*, middle panel). Interestingly, these $GAL3^+$ macrophages often exhibited an amoeboid shape (Fig. 3*A*, middle panel, *C*,*D*,*F*), suggestive of an activated state. TEM analysis (Fig. 3*E*) revealed ultrastructural features of an activated macrophage-like cell. Dual immunostaining for GAL3 and CD68, a well-known

←

panel) and aged (right panel) LW (see detailed information in Extended Data Fig. 2-2). ***L***, Genes linked to human deafness are differentially expressed in middle-aged and aged LW (see detailed information in Extended Data Fig. 2-3). The reference list of ~700 genes involved in human deafness was obtained from Lewis et al. (2022). ***M***, ***N***, $IBA1^+$ macrophages (arrows) in the AN region show no significant changes in the middle-aged cochleas compared with cochleas in young adult mice. Scale bars: 20 μm in ***A***; 30 μm in ***C***; 20 μm in ***F***; and 20 μm in ***J*** and ***N*** (applies to ***I***, ***J***, ***M***, ***N***).

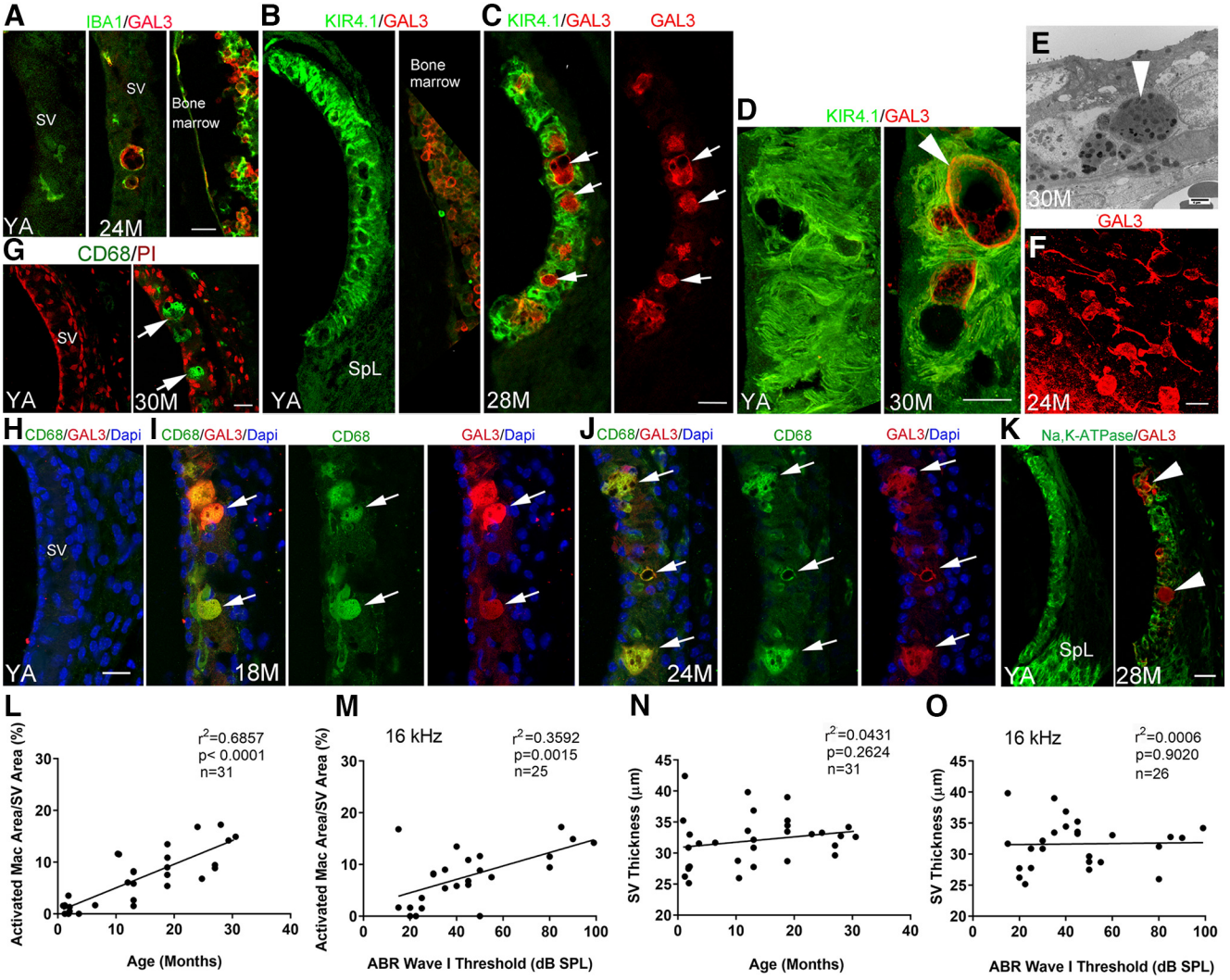

Figure 3. Macrophage dysfunction in the SV, but not SV thickness, is associated with age and ABR Wave I thresholds in CAB/CaJ mice. ***A***, Immunohistochemical analysis of IBA1 (macrophages) and the inflammation marker Galectin3 (GAL3) showed that activated macrophages expressed GAL3 in the SV of aged mice. The right panel illustrates dual staining for IBA1 and KIR4.1 in bone marrow of the same YA mouse used for the image in the left panel. ***B***, ***C***, Dual-immunostaining for KIR4.1 and GAL3 revealed limited if any colocalization in the SV of the YA mice. In the SV of aged mice, an increase in $GAL3^+$ cells (arrows) was present between but not within the $KIR4.1^+$ cellular processes of intermediate cells. ***D***, High-resolution images of the SV in YA and aged (30 M) mice revealed $GAL3^+$ macrophages (arrowhead) with large melanosome-like dark inclusions. ***E***, Ultrastructural image of the SV in an aged mouse showed a macrophage-like cell with lysosome-like bodies (arrowhead) and numerous dark inclusions comparable to the cellular changes in the $GAL3^+$ macrophages seen in ***D***. ***F***, Many $GAL3^+$ activated macrophages were seen in the SV of aged mice in whole-mount preparations. ***G***, Macrophages in the SV of an aged mouse were positive for CD68 (arrows). ***H–J***, Dual-immunostaining of CD68 and GAL3 detects $CD68^+/GAL3^+$ activated macrophages (arrows) in middle-aged (***I***) and aged (***J***) mice but not in YA mice (***H***). ***K***, $GAL3^+$ cells (arrowheads) are increased in aged mice SV, but these cells were associated with diminished staining for Na,K-ATPase (α subunit). ***L–O***, Linear regression analyses (see statistical results included in graphs in ***L–O***) revealed a significant age-dependent and ABR Wave I threshold-dependent association with area occupied by activated macrophages in the middle portion of the SV in CBA/CaJ mice. In contrast, neither mouse age nor ABR Wave I threshold was significantly associated with SV thickness. Scale bars: 20 µm in ***A***, ***G***, ***F***; 20 µm in ***C*** (applies to ***B***, ***C***); 20 µm in ***H*** (applies to ***H–J***); 25 µm in ***K***; 10 µm ***D***; and 4 µm in ***E***.

activated macrophage/microglia marker (Unger et al., 2018), revealed strong immunoreactivity for CD68 in amoeboid-like shapes (Fig. 3*G*) that co-expressed GAL3 (Fig. 3*I*,*J*) in the SV of both middle-aged and aged mice. No $GAL3^+/KIR4.1^+$ or $GAL3^+$/Na,K-$ATPase^+$ cells were identified in the young adult cochlea (Fig. 3*B*,*K*, left panel). As shown in Figure 3*B*,*K*, in the young adult cochlea, $KIR4.1^+$ elongated intermediate cell processes and Na,K-$ATPase^+$ marginal cell processes predominately occupied areas of the SV needed for maintenance of cochlear ion homeostasis. In contrast, in the aged cochlea, $GAL3^+$ activated macrophages occupied a large portion of the strial area, normally occupied by ion channel-expressing strial cells. The percentage of strial area occupied by activated macrophages and the SV thickness (reviewed earlier) were calculated in the middle turn of young, middle-aged, and aged mice. Linear regression analysis revealed a significant positive correlation between the area occupied by activated macrophages and age but no relationship between SV thickness and age (Fig. 3*L*,*N*). We further demonstrated a significant positive correlation between activated macrophage area and ABR Wave I thresholds but found no association between SV thickness and ABR thresholds (Fig. 3*M*,*O*).

Age-related dysregulation of macrophages isolated from the *Cx3cr1*$^{GFP/+}$ mouse cochlea

To test the hypothesis that activated macrophages are dysfunctional and dysregulated in the aging cochlea, we examined transcriptional profiles of macrophages isolated from the cochlea at

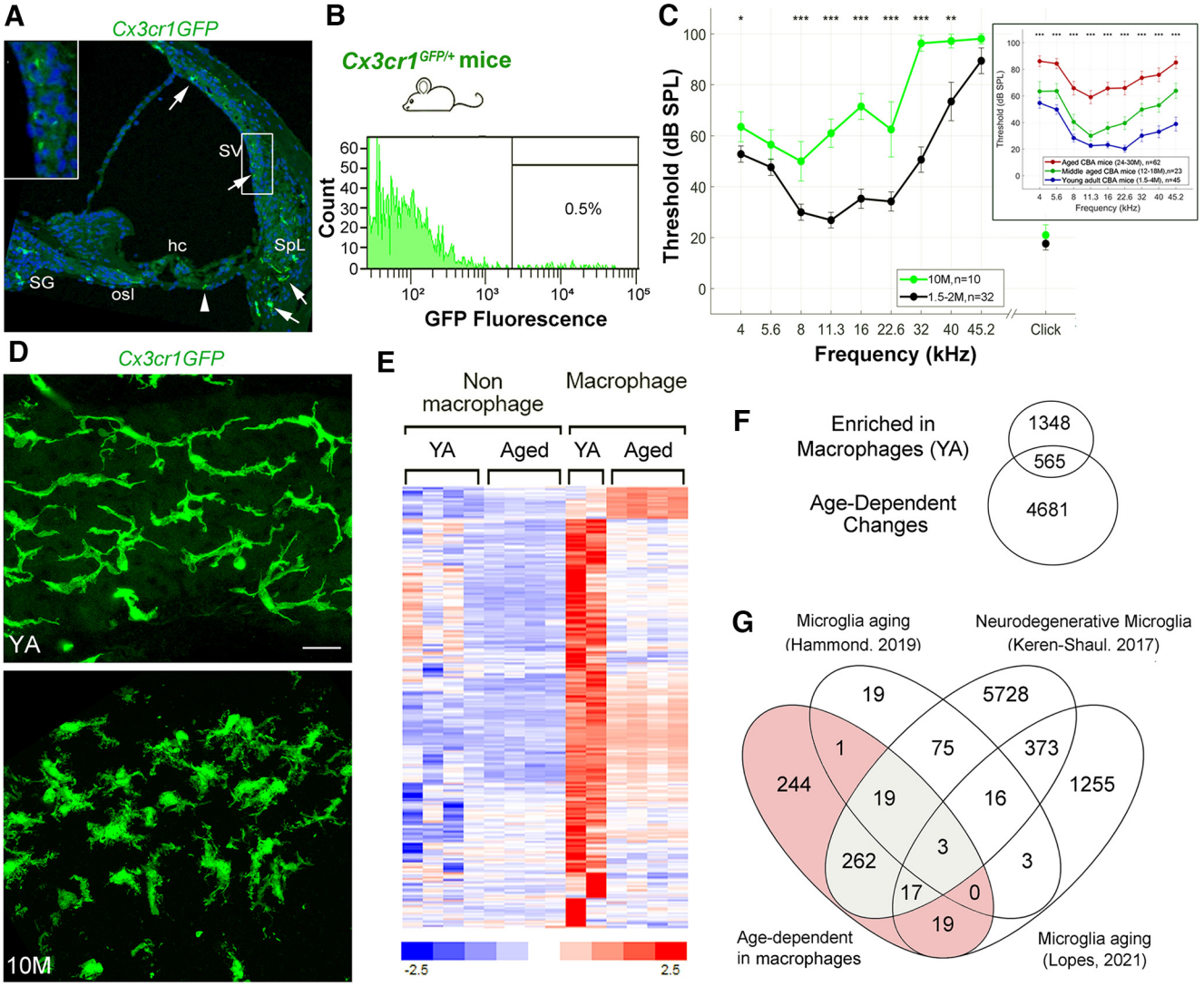

Figure 4. Dysfunction/dysregulation of macrophages in the aged mouse cochlea. ***A***, A confocal micrograph demonstrates the distribution of macrophages (GFP, green) in the cochlea of a young adult (YA) *Cx3cr1*$^{GFP/+}$ mouse. Arrows identify Cx3cr1^{+} cells in the SV, spiral ligament (SpL), osseous spiral lamina (osl), and spiral ganglion (SG). Left-top panel, Enlarged image of the boxed area in the SV. An arrowhead indicates a Cx3cr1^{+} cell in the tympanic covering layer under the organ of Corti. Nuclei were counterstained with DAPI (blue). Hair cell; hc. ***B***, A representative frequency histogram of the proportion of cells sorted from the cochlea (AN and LW portion combined) of adult *Cx3cr1*$^{GFP/+}$ mice, demonstrating the fraction (0.5%) of macrophages harvested via fluorescence-activated cell sorting (FACS). ***C***, Analysis of ABR Wave I thresholds in *Cx3cr1*$^{GFP/+}$ mice demonstrates that loss of hearing sensitivity occurs in 10-M-old relative to YA (1.5–2 M) animals. ***D***, Confocal micrographs of the SV of a 2-M-old and a 10-M-old *Cx3cr1*$^{GFP/+}$ mouse. Scale bar: 20 μm in ***D***. ***E***, ***F***, Identification of 565 genes significantly differentially expressed between YA macrophages and nonmacrophage cells and between macrophages from YA and aged mouse cochlea. Venn diagram in ***F*** represents the significant differentially expressed genes found to (1) be enriched in macrophages from YA mice, 1913 genes; and (2) demonstrate an age-dependent change, 5146 genes. Hierarchical clustering of the 565 genes illustrates the change in gene expression with age, where a small subset exhibits upregulation in the aged macrophage samples and the remaining genes are downregulated when compared with macrophages from YA mice (***E***; Extended Data Fig. 4-1). ***G***, Venn diagram showing the overlap between the 565 significant macrophage molecular markers (shaded; listed as "Age-dependent in macrophages") and genes reported in other studies as macrophage/microglia markers linked to aging or disease (Keren-Shaul et al., 2017; Hammond et al., 2019; Lopes et al., 2022). A total of 321 of the 565 were indicated in at least one of the studies (Extended Data Fig. 4-1). Gray shaded region highlights 301 genes reported as biomarkers for disease-associated microglia (Keren-Shaul et al., 2017). Scale bar, 20 μm in ***D***.

different ages. *Cx3cr1*$^{GFP/+}$ (*CX3CR1-GFP* heterozygous) mice, which express EGFP in brain microglia, macrophages, and other immune cells under the control of the endogenous *Cx3cr1* locus (Burgess et al., 2019); have previously been employed for studies of cochlear macrophages (Claussen et al., 2022; Sautter et al., 2006; Shin et al., 2022). Using these mice, we first examined the distribution of GFP^{+} cells in the young adult cochlea. Figure 4*A* illustrates the appearance of GFP^{+} cells in the SV, in the spiral ligament, and within Rosenthal's canal and the osseous spiral lamina of a *Cx3cr1*$^{GFP/+}$ mouse. No GFP^{+} cells were seen within the organ of Corti, but a small number of GFP^{+} cells were present within the tympanic-covering layer (around the tympanic border cells). The *Cx3cr1*$^{GFP/+}$ model is on a C57BL/6 genetic background and therefore could have a different temporal profile of hearing loss compared with CBA/CaJ mice. Analysis of hearing sensitivity in *Cx3cr1*$^{GFP/+}$ mice at 10 months showed a moderate-to-severe elevation of ABR Wave I thresholds compared with young adults ($F_{(1,10)}$ = 5.76, p = 0.019; Fig. 4*C*). Additionally, at 10 months, macrophages in the SV showed morphologic alterations similar to those observed in middle-aged and aged CBA/CaJ mice (Fig. 4*D*). We, therefore, chose 12- to 14-month-old *Cx3cr1*$^{GFP/+}$ mice as a representation of an aged state (aged *Cx3cr1*$^{GFP/+}$ mice) based on the observed hearing deficiencies and the evident macrophage morphologic alterations.

RNA-seq analysis was performed on macrophage and nonmacrophage cell populations isolated from young adult (1.5–2 months) and aged *Cx3cr1*$^{GFP/+}$ mice via fluorescence-activated cell sorting (Fig. 4*B*). Comparison of macrophages to nonmacrophage cells of young adult mice identified 1913 genes that were significantly upregulated in the macrophage samples (fold change increase $>$ 2, *p*-adjusted $<$ 0.05; Fig. 4*E*; Extended Data Fig. 4-1). These genes included many well-established markers of macrophage identity and function, such as *Itgam* (Cd11b), *Aif1* (IBA-1), *Cd68*, *Cd80*, *Cd163*, *Fcer1g*, *Siglec1*, *Irf5*, and *Cx3cr1*, thereby confirming the identity of the macrophage population and validating our cell isolation procedure. Of the 1913 genes enriched in macrophages in young adult mice, 565 (30%) were differentially expressed between macrophages from young adult and aged samples, suggesting that a substantial number of macrophage associated genes were affected by the aging process. Most of these genes were downregulated, supporting the hypothesis that aging is accompanied by diminished macrophage function. A subset of these 565 genes (321 genes; 57%) have been reported previously to be related to macrophage/microglia in aging or disease (Extended Data Fig. 4-1; Keren-Shaul et al., 2017; Hammond et al., 2019; Lopes et al., 2022). Notably, 301 genes from this list have been described as biomarkers of a novel type of microglia associated with neurodegenerative disease (Keren-Shaul et al., 2017; Deczkowska et al., 2018). Together, these results support the hypothesis that increased macrophage activation in the cochlea is a result of macrophage aging and/or dysfunction/dysregulation.

Increased macrophage activation in the cochlea of human temporal bones from older donors

Significant spatial and temporal differences have been identified in the behavior of macrophages/microglia in the human central nervous system compared with that in mouse models, especially in the pathologic conditions associated with aging and other neurodegenerative diseases (Smith and Dragunow, 2014; Galatro et al., 2017; Böttcher et al., 2019). As such, we examined cochlear tissues from an age-graded array of human temporal bones from 24 donors (aged 20–89+ years) for evidence of age-related macrophage dysfunction. Lectin histochemical approaches have been used widely to visualize glycoconjugates (oligosaccharides) related to different cell types and cellular components (e.g., vascular endothelial cells in mammals including mouse strial capillaries; Spicer and Schulte, 1988, 1992; Meyer et al., 2008; Neng et al., 2015; Fig. 2). Using a specific lectin, *Ulex europaeus* agglutinin I (UEA I) that interacts selectively with human endothelial cells (Holthöfer et al., 1982), we optimized a histochemical approach to visualize microvasculature in both whole-mounts and sections of human cochlear tissues (Figs. 5, 6). In whole-mount preparations from temporal bones from young adult donors, UEA I selectively stained strial microvasculature in human cochlea (Fig. 5*A*–*C*). Dual histochemical staining of whole-mounts with UEA I and IBA1 revealed the strial microvasculature and macrophages with many cellular processes (Fig. 5*B*), although a low signal-to-background ratio was observed in some whole-mounts (Fig. 5*A*). To overcome this technical limitation, we evaluated the pattern of the interaction between the IBA$^+$ macrophages with the UEA I$^+$ SV microvasculature by (1) examining cellular interactions in cochlear sections (Fig. 5*D*,*E*) and (2) enhancing the IBA1 signal on macrophages by labeling IBA1 with both Fluorescein-conjugated and Texas Red-conjugated secondary antibodies (Fig. 5*H*). Examination of a whole-mount preparation of a temporal bone from a 31-year-old male donor (Fig. 5*B*,*H*) was conducted together with cochlear sections of temporal bones from a total of six donors ranging in age from 20–42 years (five males and one female; the postmortem fixation interval ranged 7–24 h; Fig. 5*D*–*F*) revealed a close interaction between elongated cellular processes of the IBA$^+$ macrophages and the UEA I$^+$ microvasculature, an observation similar to that seen in young adult CBA/CaJ mice. Dual histochemical staining using UEA I and the anti-GAL3 macrophage activation marker on cochlear sections from young adult human donors showed few or no GAL3$^+$ cells contacting the strial microvasculature (Fig. 5*F*), similar to the staining pattern in the young adult mice (Fig. 3*A*).

In whole-mount LW preparations from the temporal bone of a middle-age donor (age 58; female), we observed activated macrophages in the SV. As shown in Figure 6*A*,*B*, numerous macrophages were present with an amoeboid shape and a reduced association with the UEA I$^+$ strial microvasculature. This observation was supported by quantitative analysis of activated macrophages in SV sections from six 55- to 65-year-old donors (three males and three females; the postmortem fixation interval ranged 6–16 h; Fig. 6*D*,*J*–*L*). GAL3$^+$ cells also were seen in the SV of a middle-aged donor (age 57; female), further supporting the interpretation that activated macrophages can be present in the human SV by middle age (Fig. 6*C*).

For the analysis of aged cochlear tissues, we included temporal bones from 12 older donors (aged 65–89+; six males and six females; the postmortem fixation interval ranged 3–35 h). Dual-staining of whole-mount preparations from an older donor with UAE I and anti-IBA1 revealed a reduction in strial microvasculature and increased macrophage activation (Fig. 6*E*,*F*). Age-related changes in human strial microvasculature were also examined using the persistent homology approach, which demonstrated a loss of SV branching in older donors (Fig. 7), similar to that seen in the aged CBA/CaJ mice (Fig. 2*G*). The SV of cochleas from older donors contained large GAL3$^+$ cell bodies showing little if any contact with the UEA I$^+$ microvasculature (Fig. 6*H*), suggesting a reduced interaction between activated macrophages and the strial microvasculature. Consistent with these observations, quantitative analysis of IBA$^+$ macrophages in middle-turn SV sections from these 12 older donors showed increased macrophage activation as compared with cochleas from young adult donors (Fig. 6*I*,*J*). Linear regression analyses were conducted for macrophage activity, strial thickness, and strial microvasculature density (UEA I$^+$ capillaries per SV section) in middle turn sections from 24 temporal bones including six younger (age 20–42; five males), six middle-aged (age 55–65; three males), and 12 older (age 68 to $>$89; six males) donors. Consistent with the findings in CBA/CaJ mice described above, a significant positive association was observed between the number of activated macrophages and age at donation (Fig. 6*J*). Also consistent with the findings in the mouse model (inset), no significant correlation was observed between SV thickness in the middle turn and donor age (Fig. 6*K*; simple linear regression; see statistical results included in Fig. 6*K*). Finally, no significant correlation was observed between microvasculature counts in the middle turn and donor age (Fig. 6*L*; simple linear regression; see statistical results included in Fig. 6*L*).

Discussion

Age-related hearing loss is a progressive disorder resulting from a decrease in function and in some cases the complete loss of

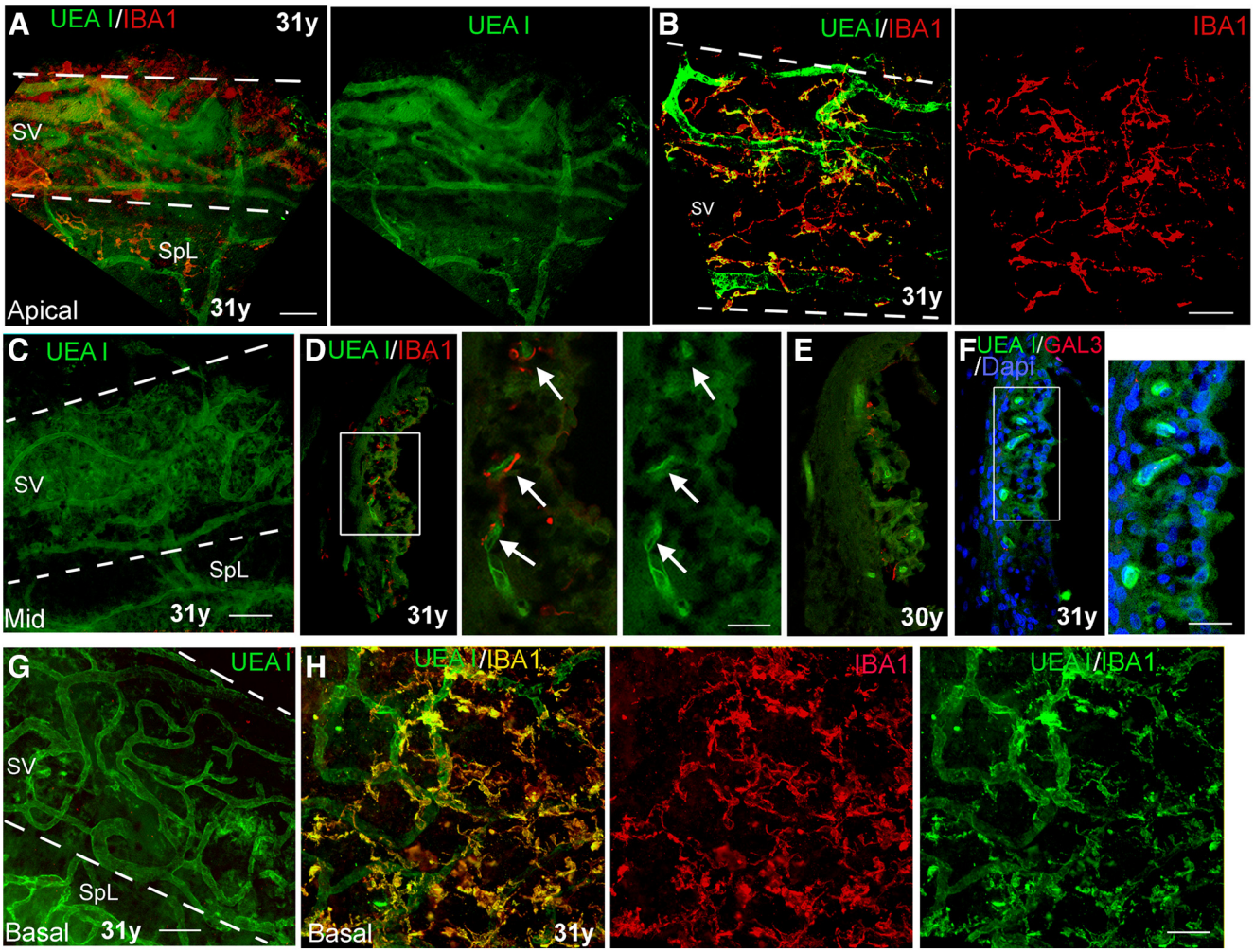

Figure 5. A lectin histochemical approach to visualize interactions between macrophages and SV microvasculature in cochleas from human temporal bones from young adult donors. ***A***, ***B***, Dual staining with UEA I and anti-IBA1 in a whole-mount preparation of a temporal bone from a young adult donor. The images taken from the apical turns (***A***, ***B***) revealed IBA1$^+$ macrophages (red) and UEA I$^+$ microvasculature network. The strial area is highlighted with two dotted lines. SpL, spiral ligament. ***C***, UEA I$^+$ microvasculature network in the middle turn of the temporal bone from the same donor. ***D***, ***E***, Dual staining of UEA I and anti-IBA1 on the sections of temporal bones from young adult donors clearly show the cellular processes of the IBAI$^+$ macrophages closely opposed to UEA I$^+$ strial microvasculature (arrows). ***D***, Central panel, Enlarged image of the boxed area in the left panel. ***F***, No strial cells stained positively with the macrophage activation marker GAL3. ***F***, Right panel, Enlarged image of the boxed area in ***F***. Note that there are GAL3$^+$ cells in the SV from the temporal bones from middle-aged and older donors (see Fig. 6). ***G***, UEA I$^+$ microvasculature in the SV of the basal turn from the temporal bone from a young adult donor. ***H***, Interactions of IBA1$^+$ macrophages (yellow) with UEA I$^+$ microvasculature (green) were visualized in the basal turn from the temporal bone from a young adult donor. Scale bars: 50 μm in ***A–C***, ***G***, ***H***; 20 μm in right panels in ***D***, ***F***.

multiple neural and non-neural elements of the cochlea, together with dysregulation of the immune system (Frisina and Walton, 2006; Lauer et al., 2012; Liberman and Liberman, 2019; Keithley, 2020, 2022; Celaya et al., 2021; Noble et al., 2022). In late adulthood, degeneration can occur in most cell types within the cochlea. Identifying the early pathophysiological events is a critical step in determining the biological mechanisms involved in age-related hearing loss. Here, we employed a mouse model of "normal" age-related hearing loss, together with analysis of human temporal bones, to demonstrate that increased macrophage activation and SV dysfunction are early events in cochlear aging. These results provide new insights into the timing of age-related pathophysiology and the underpinnings of macrophage-associated age-related cochlear degeneration. Importantly, methodological improvement and a novel approach to structural and functional evaluation of the cochlear LW allowed us to directly compare pathologic alterations in the SV of a mouse model of presbyacusis with those from human temporal bone specimens.

Inflammaging and macrophage activation in the SV begins in middle age in mouse and human

The complex structure and high metabolic activity of the SV are likely to render it susceptible to stress-associated and age-associated damage. An important finding of this study is that the molecular and cellular alterations in the LW of middle-aged CBA/CaJ mice are occurring at a time that precedes significant loss of sensory hair cells and spiral ganglion neurons, which has been reported in numerous prior studies (Spongr et al., 1997; Kujawa and Liberman, 2006; Ohlemiller et al., 2010). Transcriptomic analysis of the middle-aged LW detected changes in gene expression indicative of inflammaging, which can be triggered by harmful signals, such as certain cytokines. When detected, these signals should result in the activation of inflammasomes and other harmful signaling cascades. In the middle-aged mouse SV, we detected upregulation of proinflammatory molecules, including *Lgals3*, *Cd84*, *Itgb2*, and *Wnt5a*. Based on these findings, it is highly probable that these and other pathologic alterations identified in the SV of middle-aged CBA/CaJ mice such as

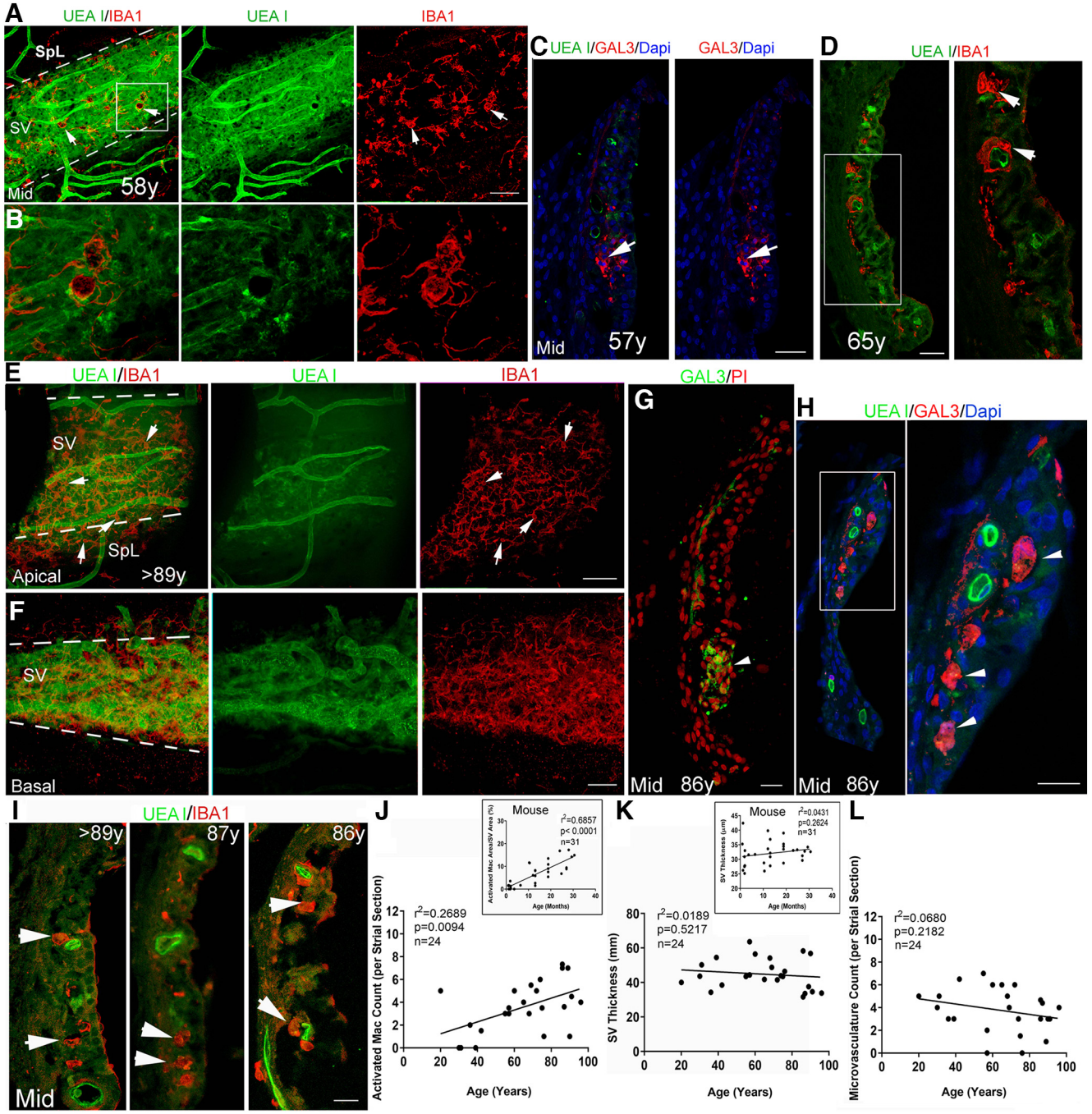

Figure 6. Increased macrophage activation in the SV from temporal bones from middle-aged and older donors. ***A***, ***B***, Dual staining with UEA I and anti-IBA1 in whole-mount preparations in a temporal bone from a middle-aged donor. The image from the middle turn reveals increased IBA1$^+$ macrophage (red) activation and a disrupted interaction of macrophages with the UEA I$^+$ microvasculature (green). Strial area is highlighted by two dotted lines. ***B***, Enlarged image of the boxed area in ***A***. ***C***, GAL3$^+$ cells (arrows) in the SV of the LW in a temporal bone from another middle-aged donor. ***D***, IBA1$^+$ macrophages with an amoeboid shape (arrows) were seen in the SV of a temporal bone from a middle-aged donor. Right panel, Enlarged image of the boxed area in the left panel. ***E***, ***F***, Dual staining with UEA I and anti-IBA1 in whole-mount preparations from a temporal bone from an older donor. Images from the LW in the apical (***E***) and basal (***F***) turn revealed a reduction of UEA I$^+$ microvasculature in the apical turn. This age-related strial microvasculature difference was confirmed using the persistent homology approach (Fig. 7). Increased IBA1$^+$ macrophage (red) activation was seen in both apical and basal turns. Arrows identify macrophages with an amoeboid-shaped cell body and fewer elongated cellular processes. ***G***, ***H***, GAL3$^+$ cells (arrows) were identified in the SV of the LW section in the temporal bone from another older donor. ***I–L***, An increase in IBA1$^+$ macrophages with an amoeboid shape (arrowheads) is seen in the SV from temporal bones from three older donors compared with that in temporal bones from young adult donors in Figure 5*D*,*E*. This observation is supported by linear regression analyses, which revealed a significant age-dependent increase in activated macrophages in the middle turn SV (main image in ***J***). There was no significant correlation between UEA I$^+$ microvasculature count in the middle turn and age at donation ($p > 0.05$). Scale bars: 50 µm in ***A***; 50 µm in ***E***, ***F***; 20 µm in ***C***, ***D***, ***G***, ***H***, right panel, ***I***.

the reduced ion channel expression in intermediate cells, could all be driven by inflammation. Increased macrophage activation has been directly associated with the release of inflammasome components (Mamik and Power, 2017). The onset of strial pathology and the alterations in expression of inflammaging-related genes, particularly the upregulation of proinflammatory markers, suggest that this is an early, if not an initial, event of age-related cochlear degeneration. Complementing the molecular and pathophysiological observations shown here in the SV, a recent genome-wide association meta-analysis provides molecular evidence supporting

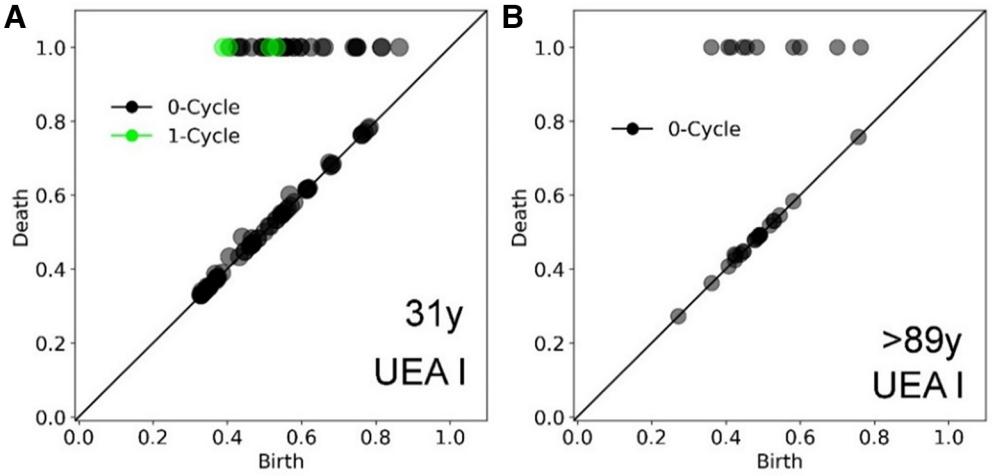

Figure 7. Differences in strial microvascular between whole-mount preparations from younger and older adult donors. Persistent homology was performed using representations of the UEA I^+-stained images of whole-mount preparations (Figs. 5*A*, 6*E*). ***A***, ***B***, Results from the temporal bone from a younger adult donor (***A***) demonstrated one-cycle loop structures representing connected vessels, as in the young adult CBA/CaJ mouse (Fig. 2*G*, left panel). In contrast, results from the temporal bone from the older adult donor (***B***) did not show one-cycle looping structures, as in the aged mouse (Fig. 2*G*, right panel). Values along the *x*- and *y*-axes are relative units after scaling by maximal death value from each analysis.

the important role of the SV in hearing impairment in humans (Trpchevska et al., 2022).

Regarding the transcriptomic analysis of AN and LW, as well as the evaluation of biological categories of inflammaging, we acknowledge the differences in cellular composition between these two structures must be considered. It is possible that the LW has a higher proportion of immune cells than the AN. However, the observation of abundant microvasculature within the AN by us and others (Fig. 3*M*,*N*; Jiang et al., 2019; Zhang et al., 2023) suggests that the difference in immune cell representation between these two structures may be less pronounced than might be expected. Nevertheless, the analysis approach that we employed was chosen to minimize effects of potential differences in cellular composition of the tissues. Our analysis counted the biological categories that were enriched within a structure at a given stage of aging. Thus, the detection of immune-related biological categories (and other inflammaging categories) was done in a region-specific fashion, and the findings are independent of any background differences in cellular composition and gene expression between LW and AN.

A significant feature of this study is that we compared age-related changes in macrophage morphology in the SV in mice and humans using a similar approach. Our findings revealed increased activated macrophages in the SV in conjunction with a change in the positional relationship between macrophages and strial capillaries beginning in middle-age in both mice and humans. Evidence of macrophage activation in human cochleas was recently reported (Noble et al., 2019; Liu et al., 2021). However, these observations were based primarily on immunostaining of cochlear sections, which limited the three-dimensional visualization and examination of their interaction with neighboring components. Here, using UEA I, a lectin with a high affinity for terminal α-L-fucose that interacts selectively with human endothelial cells, we have developed a new approach to visualize the strial microvasculature in conjunction with other molecular markers of human cochlear tissues. This novel approach has made it possible to simultaneously quantify pathologic changes in immune cell activity and the strial microvasculature in human cochleas, thus allowing, for the first time, a direct comparison of mouse and human data collected under similar parameters. These methodological improvements make it possible to apply advanced image analyses, such as persistent homology, for the quantification of differences in cochlear SV and cell morphology, thus providing a means for future otopathological investigations that scrutinize the role of the SV and immune cell malfunction in age-related hearing loss and other forms of sensorineural hearing loss.

Increased strial macrophage activation is an indicator of age-related declines in hearing sensitivity

Another important finding was that ABR Wave I thresholds were positively correlated with the level of macrophage activation in the SV, but not with SV thickness, which has been widely used as a measure of strial atrophy (or strial function). In this study, a comprehensive assessment of the SV with gene expression profiling, ultra-structural examination, and high-resolution imaging of strial cells immunostained with a K^+ channel marker enabled the identification of early strial pathologic alterations around middle age, before significant strial atrophy and other cochlear cell degeneration is observed. Our study highlights the importance of a comprehensive approach for the assessment of SV degeneration at functional, cellular, and molecular levels in future studies of age-related and other forms of sensorineural hearing loss. Our previous studies in animal models have established that age-related LW functional declines (i.e., a reduction of the EP) result in AN dysfunction, in particular, a decline in the activity of the low spontaneous AN fibers (Schmiedt et al., 1996, 2002; Lang et al., 2010). It is therefore crucial to further address the contribution of macrophage activation to age-related LW functional impairment and hearing loss using strial tissue-specific-gene manipulation models. In addition, sex differences in inflammation have been well documented (Di Florio et al., 2020). It is therefore important to further investigate the role of sex in age-related macrophage dysfunction and dysregulation. A limitation of the current study is that a smaller proportion of aged male animals was used compared with that of aged females because of the relatively shorter lifespan of male mice (Cheng et al., 2019).

A structure-function association analysis between macrophage activation in the SV and ABR Wave I thresholds increases suggests that strial dysfunction has a vital role in hearing impairment and points to cochlear inflammation as an important biomarker of age-related hearing loss. This is

supported, as detected here, by the upregulation of genes related to inflammation such as *Lgals3*. *Lgals3* (and the protein it encodes, GAL3) has been used recently as a diagnostic biomarker of inflammation in neurodegenerative diseases (Puigdellívol et al., 2020). Upregulation of GAL3 has been linked to the onset and progression of neurodegenerative disorders such as Alzheimer's disease (Soares et al., 2021). Notably, *Lgals3* has been reported to be associated with self-reports of hearing difficulty in humans via exome sequencing analysis in a recent study of participants in the UK Biobank (Lewis et al., 2022). *Lgals3* may also play an important role in the development and maintenance of normal function in the peripheral auditory system. A recent study reported that *Lgals3* deletion in female (but not male) mice led to a decline in hearing sensitivity and loss of outer hair cells (Zhang et al., 2022). Further study using a conditional knock-out model of *Lgals3* gene deficiency is needed to address the mechanism of *Lgals3* upregulation in age-related pathologic alterations in the SV.

Increased macrophage activity and cochlear inflammation have been seen in several animal models of sensorineural hearing loss. However, in most cases, the focus of those studies has been on the response of macrophages to the loss of hair cells and neurons. Here, we show that increased macrophage activation occurs in the SV of middle-aged CBA/CaJ mice, an age at which there is minimal loss of sensory hair cells and neurons (Spongr et al., 1997; Kujawa and Liberman, 2006; Ohlemiller et al., 2010). Increased macrophage activation in the SV starting from middle-age (or perhaps earlier) may be the result of dysfunction of the marginal cells and changes in their interaction with intermediate cells. A previous study revealed that mitochondria-related degeneration of marginal cells may lead to degeneration of the SV of aged gerbil cochleas (Spicer and Schulte, 2005). Insufficient ATP in marginal cells because of mitochondria dysfunction may trigger an alteration of the cytosolic Na^+/K^+ ratio, thus disturbing the ion homeostasis in the intrastrial space, where macrophages reside. A previous study showed that the involvement of K^+ efflux via macrophages is needed for inflammasome activation and consequent regulation of inflammation (Di et al., 2018).

Dysfunction of cochlear macrophages may be a key contributor to age-related hearing loss

Another important finding is that activated macrophages seen in the aging cochlea are dysfunctional, which provides evidence that aberrant macrophage activity may be an initial contributor to age-related hearing loss. Age-related macrophage dysfunction can exacerbate inflammation through a disproportionate synthesis of inflammatory regulators, disruption of the blood-labyrinth barrier, or inefficient clearance of cellular debris (Kaur et al., 2015a; Shi, 2016; Nyberg et al., 2019; Hirose and Li, 2019; Seicol et al., 2022; Noble et al., 2022; Hough et al., 2022). These changes in the aging cochlea may generate a toxic environment leading to the loss of sensory hair cells, neurons, and other cochlear cell types, promoting age-related auditory functional declines.

Although previous studies have demonstrated that macrophages are capable of responding to immune stimulation under many pathologic conditions (Lourbopoulos et al., 2015; Wolf et al., 2017; Blériot et al., 2020), macrophage dysfunction occurring during aging may impact the ability to modulate inflammation, thereby negatively impacting neural cell function (Minhas et al., 2021). Whether increased macrophage activation and cochlear inflammation seen in the middle-aged cochlea are solely the result of a response by "healthy" macrophages to an aging environment or the consequences of age-dependent macrophage dysfunction (or maladaptive macrophages) remains to be determined. Our RNA-seq analysis of macrophages obtained from aged mice suggests that aged cochlear macrophages are dysfunctional based on the findings that (1) a majority of genes affected by aging in macrophages are downregulated, and (2) >50% of these genes are reported as age-related or neurodegenerative disease-associated microglia/macrophage genes (Keren-Shaul et al., 2017; Hammond et al., 2019; Lopes et al., 2022). The identification of molecular signatures related to the immune response and regulation of macrophage stress response in aged mice supports our hypothesis that macrophage dysfunction occurs during aging, resulting in an exacerbated immune response in the cochlea. These changes could further promote macrophage activation and cochlear cell dysfunction leading to hearing impairment.

References

Aloisi F (2001) Immune function of microglia. Glia 36:165–179.

Bates D, Mächler M, Bolker B, Walker S (2015) Fitting linear mixed-effects models using lme4. J Stat Soft 67:48.

Bazard P, Pineros J, Frisina RD, Bauer MA, Acosta AA, Paganella LR, Borakiewicz D, Thivierge M, Mannering FL, Zhu X, Ding B (2021) Cochlear inflammaging in relation to ion channels and mitochondrial functions. Cells 10:2761.

Bermúdez-Muñoz JM, Celaya AM, García-Mato Á, Muñoz-Espín D, Rodríguez-de la Rosa L, Serrano M, Varela-Nieto I (2021) Dual-specificity phosphatase 1 (DUSP1) has a central role in redox homeostasis and inflammation in the mouse cochlea. Antioxidants (Basel) 10:1351.

Blériot C, Chakarov S, Ginhoux F (2020) Determinants of resident tissue macrophage identity and function. Immunity 52:957–970.

Bohne BA (1971) Scar formation in the inner ear following acoustical injury; sequence of changes from early signs of damage to healed lesion. PhD thesis, Washington University.

Böttcher C, Schlickeiser S, Sneeboer MAM, Kunkel D, Knop A, Paza E, Fidzinski P, Kraus L, Snijders GJL, Kahn RS, Schulz AR, Mei HE; NBB-Psy; Hol EM, Siegmund B, Glauben R, Spruth EJ, de Witte LD, Priller J (2019) Human microglia regional heterogeneity and phenotypes determined by multiplexed single-cell mass cytometry. Nat Neurosci 22:78–90.

Burgess M, Wicks K, Gardasevic M, Mace KA (2019) Cx3CR1 Expression identifies distinct macrophage populations that contribute differentially to inflammation and repair. Immunohorizons 3:262–273.

Carraro M, Harrison RV (2016) Degeneration of stria vascularis in age-related hearing loss; a corrosion cast study in a mouse model. Acta Otolaryngol 136:385–390.

Celaya AM, Sánchez-Pérez I, Bermúdez-Muñoz JM, Rodríguez-de la Rosa L, Pintado-Berninches L, Perona R, Murillo-Cuesta S, Varela-Nieto I (2019) Deficit of mitogen-activated protein kinase phosphatase 1 (DUSP1) accelerates progressive hearing loss. Elife 8:e39159.

Celaya AM, Rodríguez-de la Rosa L, Bermúdez-Muñoz JM, Zubeldia JM, Romá-Mateo C, Avendaño C, Pallardó FV, Varela-Nieto I (2021) IGF-1 haploinsufficiency causes age-related chronic cochlear inflammation and increases noise-induced hearing loss. Cells 10:1686.

Chen J, Bardes EE, Aronow BJ, Jegga AG (2009) ToppGene suite for gene list enrichment analysis and candidate gene prioritization. Nucleic Acids Res 37:W305–W311.

Cheng CJ, Gelfond JAL, Strong R, Nelson JF (2019) Genetically heterogeneous mice exhibit a female survival advantage that is age- and site-specific: results from a large multi-site study. Aging Cell 18:e12905.

Claussen AD, Quevedo RV, Kirk JR, Higgins T, Mostaert B, Rahman MT, Oleson J, Hernandez R, Hirose K, Hansen MR (2022) Chronic cochlear implantation with and without electric stimulation in a mouse model induces robust cochlear influx of $CX3CR1^{+/GFP}$ macrophages. Hear Res 426:108510.

Cunningham CD, Weber PC, Spicer SS, Schulte BA (2000) Canalicular reticulum in vestibular hair cells. Hear Res 143:69–83.

Deczkowska A, Keren-Shaul H, Weiner A, Colonna M, Schwartz M, Amit I (2018) Disease-associated microglia: a universal immune sensor of neurodegeneration. Cell 173:1073–1081.

Di A, Xiong S, Ye Z, Malireddi RS, Kometani S, Zhong M, Mittal M, Hong Z, Kanneganti TD, Rehman J, Malik AB (2018) The TWIK2 potassium

efflux channel in macrophages mediates NLRP3 inflammasome-induced inflammation. Immunity 49:56–65.e4.
Di Florio DN, Sin J, Coronado MJ, Atwal PS, Fairweather D (2020) Sex differences in inflammation, redox biology, mitochondria and autoimmunity. Redox Biol 31:101482.
Dufek B, Meehan DT, Delimont D, Samuelson G, Madison J, Shi X, Boettcher F, Trosky V, Gratton MA, Cosgrove D (2020) Pericyte abnormalities precede strial capillary basement membrane thickening in alport mice. Hear Res 390:107935.
Eckert MA, Harris KC, Lang H, Lewis MA, Schmiedt RA, Schulte BA, Steel KP, Vaden KI Jr, Dubno JR (2021) Translational and interdisciplinary insights into presbyacusis: a multidimensional disease. Hear Res 402:108109.
Edelsbrunner H, Letscher D, Zomorodian A (2000) Topological persistence and simplification. Proc 41st An Symp Found Comput Sci 454–63, 12-14 November, CA, IEEE.
El Kharbili M, Aviszus K, Sasse SK, Zhao X, Serban KA, Majka SM, Gerber AN, Gally F (2022) Macrophage programming is regulated by a cooperative interaction between fatty acid binding protein 5 and peroxisome proliferator-activated receptor γ. FASEB J 36:e22300.
Fleischer K (1972) The aging ear: morphological aspects. HNO 20:103–107.
Franceschi C, Bonafè M, Valensin S, Olivieri F, De Luca M, Ottaviani E, De Benedictis G (2000) Inflamm-aging: an evoluationary perspective on immunosenescence. Ann N Y Acad Sci 908:244–254.
Franceschi C, Garagnani P, Parini P, Giuliani C, Santoro A (2018) Inflammaging: a new immune-metabolic viewpoint for age-related diseases. Nat Rev Endocrinol 14:576–590.
Frisina RD, Walton JP (2006) Age-related structural and functional changes in the cochlear nucleus. Hear Res 216–217:216–223.
Frisina RD, Ding B, Zhu X, Walton JP (2016) Age-related hearing loss: prevention of threshold declines, cell loss and apoptosis in spiral ganglion neurons. Aging (Albany NY) 8:2081–2099.
Frye MD, Yang W, Zhang C, Xiong B, Hu BH (2017) Dynamic activation of basilar membrane macrophages in response to chronic sensory cell degeneration in aging mouse cochleae. Hear Res 344:125–134.
Fulop T, Larbi A, Dupuis G, Le Page A, Frost EH, Cohen AA, Witkowski JM, Franceschi C (2018) Immunosenescence and inflamm-aging as two sides of the same coin: friends or foes? Front Immunol 8:1960.
Galatro TF, Holtman IR, Lerario AM, Vainchtein ID, Brouwer N, Sola PR, Veras MM, Pereira TF, Leite REP, Möller T, Wes PD, Sogayar MC, Laman JD, den Dunnen W, Pasqualucci CA, Oba-Shinjo SM, Boddeke EWGM, Marie SKN, Eggen BJL (2017) Transcriptomic analysis of purified human cortical microglia reveals age-associated changes. Nat Neurosci 20:1162–1171.
Garin A, Tauzin G (2019) A topological "reading" lesson: classification of MNIST using TDA. 18th IEEE International Conference on Machine Learning and Applications (ICMLA), pp 1551–1556, 16-19 December, FL, IEEE.
Gratton MA, Schulte BA (1995) Alterations in microvasculature are associated with atrophy of the stria vascularis in quiet-aged gerbils. Hear Res 82:44–52. PMID: 28671693
Gorący I, Grudniewicz S, Safranow K, Ciechanowicz A, Jakubiszyn P, Gorący A, Brykczyński M (2020) Genetic polymorphisms of MMP1, MMP9, COL1A1, and COL1A2 in polish patients with thoracic aortopathy. Dis Markers 2020:9567239.
Hammond TR, Dufort C, Dissing-Olesen L, Giera S, Young A, Wysoker A, Walker AJ, Gergits F, Segel M, Nemesh J, Marsh SE, Saunders A, Macosko E, Ginhoux F, Chen J, Franklin RJM, Piao X, McCarroll SA, Stevens B (2019) Single-cell RNA sequencing of microglia throughout the mouse lifespan and in the injured brain reveals complex cell-state changes. Immunity 50:253–271.e6.
Hao X, Xing Y, Moore MW, Zhang J, Han D, Schulte BA, Dubno JR, Lang H (2014) Sox10 expressing cells in the lateral wall of the aged mouse and human cochlea. PLoS One 9:e97389.
Henderson NC, Sethi T (2009) The regulation of inflammation by galectin-3. Immunol Rev 230:160–171.
Hirose K, Li SZ (2019) The role of monocytes and macrophages in the dynamic permeability of the blood-perilymph barrier. Hear Res 374:49–57.
Hirose K, Discolo CM, Keasler JR, Ransohoff R (2005) Mononuclear phagocytes migrate into the murine cochlea after acoustic trauma. J Comp Neurol 489:180–194.
Holthöfer H, Virtanen I, Kariniemi AL, Hormia M, Linder E, Miettinen A (1982) *Ulex europaeus* I lectin as a marker for vascular endothelium in human tissues. Lab Invest 47:60–66.
Hough K, Verschuur CA, Cunningham C, Newman TA (2022) Macrophages in the cochlea; an immunological link between risk factors and progressive hearing loss. Glia 70:219–238.
Imai Y, Ibata I, Ito D, Ohsawa K, Kohsaka S (1996) A novel gene iba1 in the major histocompatibility complex class III region encoding an EF hand protein expressed in a monocytic lineage. Biochem Biophys Res Commun 224:855–862.
Ito D, Imai Y, Ohsawa K, Nakajima K, Fukuuchi Y, Kohsaka S (1998) Microglia-specific localisation of a novel calcium binding protein, Iba1. Brain Res Mol Brain Res 57:1–9.
Ito T, Li X, Kurima K, Choi BY, Wangemann P, Griffith AJ (2014) Slc26a4-insufficiency causes fluctuating hearing loss and stria vascularis dysfunction. Neurobiol Dis 66:53–65.
Jiang H, Wang X, Zhang J, Kachelmeier A, Lopez IA, Shi X (2019) Microvascular networks in the area of the auditory peripheral nervous system. Hear Res 371:105–116.
Kaur T, Hirose K, Rubel EW, Warchol ME (2015a) Macrophage recruitment and epithelial repair following hair cell injury in the mouse utricle. Front Cell Neurosci 9:150.
Kaur T, Zamani D, Tong L, Rubel EW, Ohlemiller KK, Hirose K, Warchol ME (2015b) Fractalkine signaling regulates macrophage recruitment into the cochlea and promotes the survival of spiral ganglion neurons after selective hair cell lesion. J Neurosci 35:15050–15061.
Keithley EM (2020) Pathology and mechanisms of cochlear aging. J Neurosci Res 98:1674–1684.
Keithley EM (2022) Inner ear immunity. Hear Res 419:108518.
Keren-Shaul H, Spinrad A, Weiner A, Matcovitch-Natan O, Dvir-Szternfeld R, Ulland TK, David E, Baruch K, Lara-Astaiso D, Toth B, Itzkovitz S, Colonna M, Schwartz M, Amit I (2017) A unique microglia type associated with restricting development of Alzheimer's disease. Cell 169:1276–1290.e17.
Korrapati S, Taukulis I, Olszewski R, Pyle M, Gu S, Singh R, Griffiths C, Martin D, Boger E, Morell RJ, Hoa M (2019) Single cell and single nucleus RNA-Seq reveal cellular heterogeneity and homeostatic regulatory networks in adult mouse stria vascularis. Front Mol Neurosci 12:316.
Kujawa SG, Liberman MC (2006) Acceleration of age-related hearing loss by early noise exposure: evidence of a misspent youth. J Neurosci 26:2115–2123.
Kurata N, Schachern PA, Paparella MM, Cureoglu S (2016) Histopathologic evaluation of vascular findings in the cochlea in patients with presbycusis. JAMA Otolaryngol Head Neck Surg 142:173–178.
Kusunoki T, Cureoglu S, Schachern PA, Baba K, Kariya S, Paparella MM (2004) Age-related histopathologic changes in the human cochlea: a temporal bone study. Otolaryngol Head Neck Surg 131:897–903.
Lang H, Jyothi V, Smythe NM, Dubno JR, Schulte BA, Schmiedt RA (2010) Chronic reduction of endocochlear potential reduces auditory nerve activity: further confirmation of an animal model of metabolic presbyacusis. J Assoc Res Otolaryngol 11:419–434.
Lang H, Li M, Kilpatrick LA, Zhu J, Samuvel DJ, Krug EL, Goddard JC (2011) Sox2 up-regulation and glial cell proliferation following degeneration of spiral ganglion neurons in the adult mouse inner ear. J Assoc Res Otolaryngol 12:151–171.
Lang H, Xing Y, Brown LN, Samuvel DJ, Panganiban CH, Havens LT, Balasubramanian S, Wegner M, Krug EL, Barth JL (2015) Neural stem/progenitor cell properties of glial cells in the adult mouse auditory nerve. Sci Rep 5:13383.
Lauer AM, Fuchs PA, Ryugo DK, Francis HW (2012) Efferent synapses return to inner hair cells in the aging cochlea. Neurobiol Aging 33:2892–2902.
Lawson P, Sholl AB, Brown JQ, Fasy BT, Wenk C (2019) Persistent homology for the quantitative evaluation of architectural features in prostate cancer histology. Sci Rep 9:1139.
Liberman LD, Liberman MC (2019) Cochlear efferent innervation is sparse in humans and decreases with age. J Neurosci 39:9560–9569.
Lewis MA, Schulte BA, Dubno JR, Steel KP (2022) Investigating the characteristics of genes and variants associated with self-reported hearing difficulty in older adults in the UK Biobank. BMC Biol 20:150.
Liu H, Giffen KP, Chen L, Henderson HJ, Cao TA, Kozeny GA, Beisel KW, Li Y, He DZ (2022) Molecular and cytological profiling of biological aging of mouse cochlear inner and outer hair cells. Cell Rep 39:110665.

Liu T, Li G, Noble KV, Li Y, Barth JL, Schulte BA, Lang H (2019) Age-dependent alterations of Kir4.1 expression in neural crest–derived cells of the mouse and human cochlea. Neurobiolo Aging 80:210–222.

Liu W, Molnar M, Garnham C, Benav H, Rask-Andersen H (2018) Macrophages in the human cochlea: saviors or predators—a study using super-resolution immunohistochemistry. Front Immunol 9:223.

Liu W, Danckwardt-Lilliestrom N, Schrott-Fischer A, Glueckert R, Rask-Andersen H (2021) Distribution of immune cells including macrophages in the human cochlea. Front Neurol 12:781702.

Lopes KdP, Snijders GJL, Humphrey J, Allan A, Sneeboer MAM, Navarro E, Schilder BM, Vialle RA, Parks M, Missall R, van Zuiden W, Gigase FAJ, Kübler R, van Berlekom AB, Hicks EM, Böttcher C, Priller J, Kahn RS, de Witte LD, Raj T (2022) Genetic analysis of the human microglial transcriptome across brain regions, aging and disease pathologies. Nat Genet 54:4–17.

Lourbopoulos A, Ertürk A, Hellal F (2015) Microglia in action: how aging and injury can change the brain's guardians. Front Cell Neurosci 9:54.

Love MI, Huber W, Anders S (2014) Moderated estimation of fold change and dispersion for RNA-seq data with DESeq2. Genome Biol 15:550.

Ma B, Zhou Y, Liu R, Zhang K, Yang T, Hu C, Gao Y, Lan Q, Liu Y, Yang X, Qi H (2021) Pigment epithelium-derived factor (PEDF) plays anti-inflammatory roles in the pathogenesis of dry eye disease. Ocul Surf 20:70–85.

Makary CA, Shin J, Kujawa SG, Liberman MC, Merchant SN (2011) Age-related primary cochlear neuronal degeneration in human temporal bones. J Assoc Res Otolaryngol 12:711–717.

Marcus DC, Wu T, Wangemann P, Kofuji P (2002) KCNJ10 (Kir4.1) potassium channel knockout abolishes endocochlear potential. Am J Physiol Cell Physiol 282:C403–C407.

Mamik MK, Power C (2017) Inflammasomes in neurological diseases: emerging pathogenic and therapeutic concepts. Brain 140:2273–2285.

Mészáros Á, Molnár K, Nógrádi B, Hernádi Z, Nyúl-Tóth Á, Wilhelm I, Krizbai IA (2020) Neurovascular inflammaging in health and disease. Cells 9:1614.

Meyer W, Godynicki S, Tsukise A (2008) Lectin histochemistry of the endothelium of blood vessels in the mammalian integument, with marks on the endothelial glycocalyx and blood vessel system nomenclature. Ann Anat 190:264–276.

Minhas PS, et al. (2021) Restoring metabolism of myeloid cells reverses cognitive decline in ageing. Nature 590:122–128.

Neng L, Zhang J, Yang J, Zhang F, Lopez IA, Dong M, Shi X (2015) Structural changes in the strial blood-labyrinth barrier of aged C57BL/6 mice. Cell Tissue Res 361:685–696.

Noble K, Brown L, Elvis P, Lang H (2022) Cochlear immune response in presbyacusis: a focus on dysregulation of macrophage activity. J Assoc Res Otolaryngol 23:1–16.

Noble KV, Liu T, Matthews LJ, Schulte BA, Lang H (2019) Age-related changes in immune cells of the human cochlea. Front Neurol 10:895.

Nyberg S, Abbott NJ, Shi X, Steyger PS, Dabdoub A (2019) Delivery of therapeutics to the inner ear: the challenge of the blood-labyrinth barrier. Sci Transl Med 11:eaao0935.

Ohlemiller KK, Rice ME, Gagnon PM (2008) Strial microvascular pathology and age-associated endocochlear potential decline in NOD congenic mice. Hear Res 244:85–97.

Ohlemiller KK, Dahl AR, Gagnon PM (2010) Divergent aging characteristics in CBA/J and CBA/CaJ mouse cochleae. J Assoc Res Otolaryngol 11:605–623.

Ohlemiller KK, Rybak-Rice ME, Rellinger EA, Ortmann AJ (2011) Divergence of noise vulnerability in cochleae of young CBA/J and CBA/CaJ mice. Hear Res 272:13–20.

Ohsawa K, Imai Y, Sasaki Y, Kohsaka S (2004) Microglia/macrophage-specific protein Iba1 binds to fimbrin and enhances its actin-bundling activity. J Neurochem 88:844–856.

Pan L, Xiao H, Liao R, Chen Q, Peng C, Zhang Y, Mu T, Wu Z (2018) Fatty acid binding protein 5 promotes tumor angiogenesis and activates the IL6/STAT3/VEGFA pathway in hepatocellular carcinoma. Biomed Pharmacother 106:68–76.

Panganiban CH, Barth JL, Darbelli L, Xing Y, Zhang J, Li H, Noble KV, Liu T, Brown LSN, Schulte BA, Richard S, Lang H (2018) Noise-induced dysregulation of Quaking RNA binding proteins contributes to auditory nerve demyelination and hearing loss. J Neurosci 38:2551–2568.

Panganiban CH, Barth JL, Tan J, Noble KV, McClaskey CM, Howard BA, Jafri SH, Dias JW, Harris KC, Lang H (2022) Two distinct types of nodes of Ranvier support auditory nerve function in the mouse cochlea. Glia 70:768–791.

Parthasarathy A, Kujawa SG (2018) Synaptopathy in the aging cochlea: characterizing early-neural deficits in auditory temporal envelope processing. J Neurosci 38:7108–7119.

Perkins G, Lee JH, Park S, Kang M, Perez-Flores MC, Ju S, Phillips G, Lysakowski A, Gratton MA, Yamoah EN (2020) Altered outer hair cell mitochondrial and subsurface cisternae connectomics are candidate mechanisms for hearing loss in mice. J Neurosci 40:8556–8572.

Puigdellívol M, Allendorf DH, Brown GC (2020) Sialylation and galectin-3 in microglia-mediated neuroinflammation and neurodegeneration. Front Cell Neurosci 14:162.

Sadanandam A, Rosenbaugh EG, Singh S, Varney M, Singh RK (2010) Semaphorin 5A promotes angiogenesis by increasing endothelial cell proliferation, migration, and decreasing apoptosis. Microvasc Res 79:1–9.

Saitoh Y, Hosokawa M, Shimada A, Watanabe Y, Yasuda N, Murakami Y, Takeda T (1995) Age-related cochlear degeneration in senescence-accelerated mouse. Neurobiol Aging 16:129–136.

Sallam T, Ito A, Rong X, Kim J, van Stijn C, Chamberlain BT, Jung ME, Chao LC, Jones M, Gilliland T, Wu X, Su GL, Tangirala RK, Tontonoz P, Hong C (2014) The macrophage LBP gene is an LXR target that promotes macrophage survival and atherosclerosis. J Lipid Res 55:1120–1130.

Sautter NB, Shick EH, Ransohoff RM, Charo IF, Hirose K (2006) CC chemokine receptor 2 is protective against noise-induced hair cell death: studies in CX3CR1(+/GFP) mice. J Assoc Res Otolaryngol 7:361–372.

Schuknecht HF (1955) Presbycusis. Trans Am Laryngol 59:401–418.

Schuknecht HF (1964) Further observations on the pathology of presbycusis. Arch Otolaryngol 80:369–382.

Schuknecht HF, Gacek MR (1993) Cochlear pathology in presbycusis. Ann Otol Rhinol Laryngol 102:1–16.

Schmiedt RA, Mills JH, Boettcher FA (1996) Age-related loss of activity of auditory-nerve fibers. J Neurophysiol 76:2799–2803.

Schmiedt RA, Lang H, Okamura HO, Schulte BA (2002) Effects of furosemide applied chronically to the round window: a model of metabolic presbyacusis. J Neurosci 22:9643–9650.

Schulte BA (2005) Inner ear K+ recycling pathways. In: Proceedings of the 5th international symposium on Meniere's disease and inner ear homeostasis disorders (Lim DJ, ed), pp 68–72. Los Angeles: Ear Institute.

Schulte BA, Schmiedt RA (1992) Lateral wall Na,K-ATPase and endocochlear potentials decline with age in quiet-reared gerbils. Hear Res 61:35–46.

Sciacchitano S, Lavra L, Morgante A, Ulivieri A, Magi F, De Francesco GP, Bellotti C, Salehi LB, Ricci A (2018) Galectin-3: one molecule for an alphabet of diseases, from A to Z. Iran J Med Sci 19:379.

Seicol BJ, Lin S, Xie R (2022) Age-related hearing loss is accompanied by chronic inflammation in the cochlea and the cochlear nucleus. Front Aging Neurosci 14:846804.

Sha SH, Kanicki A, Dootz G, Talaska AE, Halsey K, Dolan D, Altschuler R, Schacht J (2008) Age-related auditory pathology in the CBA/J mouse. Hear Res 243:87–94.

Shi X (2016) Pathophysiology of the cochlear intrastrial fluid-blood barrier (review). Hear Res 338:52–63.

Shin SH, Yoo JE, Jung J, Choi JY, Bae SH (2022) Inflammatory monocytes infiltrate the spiral ligament and migrate to the basilar membrane after noise exposure. Clin Exp Otorhinolaryngol 15:153–159.

Shukunami C, Oshima Y, Hiraki Y (2005) Chondromodulin-I and tenomodulin: a new class of tissue-specific angiogenesis inhibitors found in hypovascular connective tissues. Biochem Biophys Res Commun 333:299–307.

Smathers RL, Petersen DR (2011) The human fatty acid-binding protein family: evolutionary divergences and functions. Hum Genomics 5:170–191.

Smith AM, Dragunow M (2014) The human side of microglia. Trends Neurosci 37:125–135.

Soares LC, Al-Dalahmah O, Hillis J, Young CC, Asbed I, Sakaguchi M, O'Neill E, Szele FG (2021) Novel Galectin-3 roles in neurogenesis, inflammation and neurological diseases. Cells 10:3047.

Spicer SS, Schulte BA (1988) Detection and differentiation of glycoconjugates in various cell types by lectin histochemistry. Basic Appl Histochem 32:307–320.

Spicer SS, Schulte BA (1992) Diversity of cell glycoconjugates shown histochemically: a perspective. J Histochem Cytochem 40:1–38.

Spicer SS, Schulte BA (2005) Pathologic changes of presbycusis begin in secondary processes and spread to primary processes of strial marginal cells. Hear Res 205:225–240.

Spongr VP, Flood DG, Frisina RD, Salvi RJ (1997) Quantitative measures of hair cell loss in CBA and C57BL/6 mice throughout their life spans. J Acoust Soc Am 101:3546–3553.

Suzuki M, Sakamoto T, Kashio A, Yamasoba T (2016) Age-related morphological changes in the basement membrane in the stria vascularis of C57BL/6 mice. Eur Arch Otorhinolaryngol 273:57–62.

Tachibana M (1999) Sound needs sound melanocytes to be heard. Pigment Cell Res 12:344–354.

Tasaki I, Spyropoulos CS (1959) Stria vascularis as source of endocochlear potential. J Neurophysiol 22:149–155.

Thulasiram MR, Ogier JM, Dabdoub A (2022) Hearing function, degeneration, and disease: spotlight on the stria vascularis. Front Cell Dev Biol 10:841708.

Tornabene SV, Sato K, Pham L, Billings P, Keithley EM (2006) Immune cell recruitment following acoustic trauma. Hear Res 222:115–124.

Trpchevska N, et al. (2022) Genome-wide association meta-analysis identifies 48 risk variants and highlights the role of the stria vascularis in hearing loss. Am J Hum Genet 109:1077–1091.

Unger MS, Schernthaner P, Marschallinger J, Mrowetz H, Aigner L (2018) Microglia prevent peripheral immune cell invasion and promote an anti-inflammatory environment in the brain of APP-PS1 transgenic mice. J Neuroinflammation 15:274.

Verschuur C, Prempeh AA, Newman TA (2014) Inflammation is associated with a worsening of presbycusis: evidence from the MRC national study of hearing. Int J Audiol 53:469–475.

Warchol ME (2019) Interactions between macrophages and the sensory cells of the inner ear. Cold Spring Harb Perspect Med 9:a033555.

Watson N, Ding B, Zhu X, Frisina RD (2017) Chronic inflammation—inflammaing—in the aging cochlea: a novel target for future presbycusis therapy. Ageing Res Rev 40:142–148.

Wenes M, Shang M, Di Matteo M, Goveia J, Martín-Pérez R, Serneels J, Prenen H, Ghesquiere B, Carmeliet P, Mazzone M (2016) Macrophage metabolism controls tumor blood vessel morphogenesis and metastasis. Cell Metab 24:701–715.

Wolf SA, Boddeke HW, Kettenmann H (2017) Microglia in physiology and disease. Annu Rev Physiol 79:619–643.

White JA, Burgess BJ, Hall RD, Nadol JB (2000) Pattern of degeneration of the spiral ganglion cell and its processes in the C57BL/6J mouse. Hear Res 141:12–18.

Wu PZ, O'Malley JT, de Gruttola V, Liberman MC (2020) Age-related hearing loss is dominated by damage to inner ear sensory cells, not the cellular battery that powers them. J Neurosci 40:6357–6366.

Wu Z, Liao F, Luo G, Qian Y, He X, Xu W, Ding S, Pu J (2021) NR1D1 Deletion induces rupture-prone vulnerable plaques by regulating macrophage pyroptosis via the NF-κB/NLRP3 inflammasome pathway. Oxid Med Cell Longev 2021:5217572.

Xing Y, Samuvel DJ, Stevens SM, Dubno JR, Schulte BA, Lang H (2012) Age-related changes of myelin basic protein in mouse and human auditory nerve. PLoS One 7:e34500.

Xu B, Chen L, Zhan Y, Marquez KNS, Zhuo L, Qi S, Zhu J, He Y, Chen X, Zhang H, Shen Y, Chen G, Gu J, Guo Y, Liu S, Xie T (2022) The biological functions and regulatory mechanisms of fatty acid binding protein 5 in various diseases. Front Cell Dev Biol 10:857919.

Yu CW, Liang X, Lipsky S, Karaaslan C, Kozakewich H, Hotamisligil GS, Bischoff J, Cataltepe S (2016) Dual role of fatty acid-binding protein 5 on endothelial cell fate: a potential link between lipid metabolism and angiogenic responses. Angiogenesis 19:95–106.

Zhang C, Frye MD, Sun W, Sharma A, Manohar S, Salvi R, Hu BH (2020) New insights on repeated acoustic injury: augmentation of cochlear susceptibility and inflammatory reaction resultant of prior acoustic injury. Hear Res 393:107996.

Zhang C, Adler HJ, Manohar S, Salvi R, Sun W, Ye M, Hu BH (2022) Galectin-3 protects auditory function in female mice. Hear Res 424:108602.

Zhang F, Dai M, Neng L, Zhang JH, Zhi Z, Fridberger A, Shi X (2013) Perivascular macrophage-like melanocyte responsiveness to acoustic trauma–a salient feature of strial barrier associated hearing loss. FASEB J 27:3730–3740.

Zhang Y, Neng L, Sharma K, Hou Z, Johnson A, Song J, Dabdoub A, Shi X (2023) Pericytes control vascular stability and auditory spiral ganglion neuron survival. Elife 12:e83486.

Zheng Z, Chen Y, Wang Y, Li Y, Cheng Q (2021) MicroRNA-513b-5p targets COL1A1 and COL1A2 associated with the formation and rupture of intracranial aneurysm. Sci Rep 11:14897.